nature reviews bioengineering

https://doi.org/10.1038/s44222-024-00240-y

Review article

Check for updates

Clinical translation of photoacoustic imaging

Jeongwoo Park[1,2,3,15], Seongwook Choi[2,4,15], Ferdinand Knieling[5,15], Bryan Clingman[6], Sarah Bohndiek[7,8] ✉, Lihong V. Wang[9,10] ✉ & Chulhong Kim[1,2,3,11,12,13,14] ✉

Abstract

Photoacoustic imaging (PAI), also known as optoacoustic imaging, is a promising biomedical imaging technique that combines the benefits of rich optical contrast and high ultrasonic spatial resolution to overcome the limited penetration depth of light in living subjects. Basic biomedical research conducted with PAI in preclinical studies has generated much interest and shown outstanding potential for clinical and commercial translation. PAI has captured morphological, functional and molecular information in studies of living animals and humans, providing intrinsic clinical indicators from early diagnosis through to treatment monitoring. This Review presents the fundamentals of PAI technology and various clinical PAI systems and addresses key findings from pilot and clinical patient studies of human organ systems. The Review also discusses technical and non-technical challenges in clinical scenarios, emphasizes the importance of standardization in accelerating clinical translation, and summarizes the current state of the PAI regulatory process.

Sections

[1]Department of Electrical Engineering, Pohang University of Science and Technology (POSTECH), Pohang, Republic of Korea. [2]Medical Device Innovation Center, POSTECH, Pohang, Republic of Korea. [3]Department of Biomedical Convergence Science and Technology, School of Convergence, Kyungpook National University, Daegu, Republic of Korea. [4]Institute of Artificial Intelligence, POSTECH, Pohang, Republic of Korea. [5]Department of Pediatrics and Adolescent Medicine, University Hospital Erlangen, Friedrich-Alexander-Universität (FAU) Erlangen-Nürnberg, Erlangen, Germany. [6]Seno Medical Instruments, Inc., San Antonio, TX, USA. [7]Department of Physics, University of Cambridge, Cambridge, UK. [8]Cancer Research UK Cambridge Institute, University of Cambridge, Cambridge, UK. [9]Andrew and Peggy Cherng Department of Medical Engineering, California Institute of Technology (CALTECH), Pasadena, CA, USA. [10]Department of Electrical Engineering, CALTECH, Pasadena, CA, USA. [11]Department of Convergence IT Engineering, POSTECH, Pohang, Republic of Korea. [12]Department of Mechanical Engineering, POSTECH, Pohang, Republic of Korea. [13]Department of Medical Science and Engineering, POSTECH, Pohang, Republic of Korea. [14]Opticho Inc., Pohang, Republic of Korea. [15]These authors contributed equally: Jeongwoo Park, Seongwook Choi, Ferdinand Knieling. ✉e-mail: seb53@cam.ac.uk; LVW@caltech.edu; chulhong@postech.edu

Key points

- By combining optics and ultrasound, photoacoustic imaging breaks the fundamental penetration depth barrier of traditional optical imaging, providing absorption-based rich optical contrast and high ultrasonic spatial resolution in living tissues.
- Photoacoustic imaging systems are implemented in various forms to suit diagnostic purposes in clinical settings: dual-modal photoacoustic and ultrasound imaging based on conventional ultrasound imaging systems, station-based tomographic photoacoustic imaging, and mesoscopic/microscopic photoacoustic imaging.
- Photoacoustic pilot and clinical studies of human functional systems have demonstrated high potential for translating the modality into clinical practice.
- Despite the notable outcomes of photoacoustic imaging, several challenges remain: overcoming technical and non-technical limitations, standardizing image analyses, obtaining regulatory approval, and securing medical insurance coverage for its commercialization.

Introduction

Optical imaging has transformed biological and medical research by visualizing morphological, physiological and molecular features of living tissue[1–3]. Diffusive optical imaging (DOI) techniques in the near-infrared (NIR) spectral region have gained widespread usage in biomedical applications owing to their safety, versatility, real-time imaging capabilities and non-invasiveness[4]. A notable advantage of DOI is its ability to utilize the natural absorption characteristics of biological tissues, particularly the differential absorption properties of oxyhaemoglobin (HbO_2) and deoxyhaemoglobin (HbR) in the NIR wavelength range, which means that changes in blood oxygenation and blood volume within tissues can be measured without the need for exogenous contrast agents or dyes. This label-free imaging capability contributes to its non-invasiveness and safety and makes it suitable for a wide range of applications, from monitoring tissue oxygenation to assessing muscle performance. Despite the advantages, however, DOI has poor spatial resolution owing to strong light scattering within biological tissues[5].

In clinical practice, magnetic resonance imaging (MRI), X-ray computed tomography (CT), positron emission tomography (PET) and ultrasound imaging (USI) are standard tools used to screen for and diagnose illnesses, monitor treatment effectiveness, and track disease progression[6] but do have limitations. MRI, CT and PET are not usually portable and require specialized spaces. MRI and PET have particularly long examination times and high costs. CT and PET employ ionizing radiation, a potential health risk for both patients and medical staff. Furthermore, PET uses radioactive tracers as contrast agents, creating logistical issues of handling and disposal[7]. USI can overcome some of these limitations as it does not use ionizing radiation, can image in real time, is cost-effective and is portable. USI can readily image various body regions in a localized way and is commonly used in image-guided interventions, making it the preferred choice in many clinical scenarios[8,9]. Furthermore, it can also provide functional information such as blood flow (via Doppler ultrasonography[10]) and tissue stiffness (for example, elastography[11]) but it lacks molecule-specific contrast unless paired with microbubbles or other contrast agents[12].

Photoacoustic imaging (PAI), also called optoacoustic imaging, has attracted considerable attention in biomedical imaging over the past decade, emerging as a non-ionizing hybrid imaging modality that combines the high spatial resolution of USI with robust optical capabilities to visualize tissues a few millimetres to centimetres in depth[13]. PAI utilizes rich optical endogenous and exogenous contrast to provide in vivo information based on the light absorption characteristics of biological tissues[14]. The hybrid characteristics of PAI enable it to be integrated seamlessly with conventional USI systems, expanding the range of clinical applications while retaining existing USI capabilities[15]. As both PAI and USI can be simultaneously conducted in real time, PAI can provide additional qualitative or quantitative multiparametric assessments, complementing the morphological information from conventional USI[16]. Combining these modalities enhances the potential for comprehensive diagnostic evaluations in clinical practice (Table 1).

The photoacoustic effect was discovered by Alexander Graham Bell and Charles Sumner Tainter in 1880, and Bell patented its application under the name 'photophone'[17]. In the mid-twentieth century, similar physical mechanisms were applied in gas analysis studies, where the terms 'optoacoustic' or 'optic-acoustic' were first used[18,19]. Owing to confusion between the terms 'optoacoustic' and 'acousto-optic', the new term 'photoacoustic' was first introduced in 1973 in the context of the study of solid targets[20] and applied in various studies[21–24]. Since 1994, the terms 'optoacoustic' and 'photoacoustic' have been used interchangeably in biomedical imaging fields[25,26]. PAI has evolved rapidly over the past two decades in the area of biomedical imaging[27], from in vivo, small animal imaging via a conference proceedings article in 2000 (ref. 28), functional small animal imaging in a peer-reviewed journal article in 2003 (ref. 29), in vivo human imaging via a conference proceedings article in 2001 (ref. 30), to more recent clinical trials[14,31–38].

PAI has demonstrated its potential for clinical translation in morphological imaging based on endogenous contrasts (for example, haemoglobin (Hb)[39], melanin[40], nucleic acids[41,42], lipids[43] and collagen[44]) as well as in targeted molecular imaging (for example, with exogenous contrast agents[14,45]) and functional imaging (for example, oxygeneration[46,47], blood flow[48], stiffness[49], metabolism[50] and lymphatic-vessel mapping[51]). Here, we summarize the fundamental principles and characteristics of PAI in clinical PAI systems and describe key findings from clinical and pilot studies of different human organ systems. Technical and non-technical impediments to the clinical translation of PAI are discussed and we highlight the standardization efforts required for successful adoption of PAI in healthcare systems. Furthermore, we discuss the status of the regulatory process for the approval and use of PAI as medical equipment from an industrial perspective.

Fundamentals of PAI

In PAI, short-pulsed light directly irradiates biological tissue (Fig. 1a). Depending on its wavelength, the light is absorbed to varying degrees by endogenous chromophores (for example, DNA, RNA, Hb, melanin, collagen and lipids) or, if introduced, by FDA-approved exogenous contrast agents (for example, indocyanine green (ICG) and methylene blue). The absorption of each light pulse induces a rapid localized temperature increase, initiating thermal expansion and consequently generating an ultrasound wave whose origin can be identified by its time-of-flight. The ultrasound waves, known as photoacoustic waves, convey valuable information about the optical absorption properties of a tissue[13]. An ultrasound transducer (USTR) is typically employed to

Table 1 | Comparison of five medical imaging modalities

Modality	Structural	Molecular	Functional	Specialized space	Ionizing radiation	Imaging depth (in humans)	Spatial resolution (per depth)	Imaging time
Magnetic resonance imaging	High	High	High	High (magnetic field safety)	Low or none	Whole body	Medium	Low or none
Computed tomography	High	Low or none	Low or none	High (radiation safety)	High	Whole body	High	High (real time)
Positron emission tomography	High	High	High	High (radiation safety)	High	Whole body	Low or none	Low or none
Ultrasound imaging	High	Medium	High	Low or none	Low or none	>10 cm (ref. 243)	High	High (real time)
Photoacoustic imaging	High	High	High	Medium (laser safety)	Low or none	<5 cm (ref. 82)	High	High (real time)

detect the photoacoustic signals, which undergo signal processing[52], image reconstruction[53] and image processing[54] procedures to generate a cross-sectional 2D or 3D photoacoustic image display.

As the optical absorption coefficient of each target is wavelength dependent, photoacoustic contrast is spectrally determined by the excitation light. In general, a specific monochromatic light source within the ultraviolet, visible and/or NIR spectrum is used for photoacoustic excitation (Fig. 1b). In the ultraviolet region, nucleic acid bases (for example, adenine, guanine, cytosine, thymine and uracil) in DNA and RNA exhibit pronounced light absorption peaks at 260 nm (ref. 55) and aromatic amino acid residues (for example, tryptophan, tyrosine and phenylalanine) inside proteins absorb light strongly at 250–300 nm (ref. 56). Consequently, PAI in the ultraviolet spectrum can image cell nuclei and cytoplasm without exogenous chemical staining[41]. In the visible to NIR-I spectral range, Hb is highly absorptive, and thus PAI in this spectral range effectively visualizes vascular networks. This key ability enables PAI to monitor angiogenesis, map blood oxygenation and evaluate vascular morphology[57]. Other chromophores, such as melanin and exogenous contrast agents, have been exploited for PAI in the visible, NIR-I and NIR-II spectral ranges. Exogenous photoacoustic agents (for example, metallic nanomaterials, carbon-based nanomaterials, organic materials and semiconducting polymer nanoparticles) effectively improve the signal-to-noise ratio (SNR) and contrast, expanding the scope of PAI for functional imaging[14]. In clinical applications, FDA-approved exogenous agents, such as ICG and methylene blue, can be injected or taken up by the body to track or monitor their distribution via the digestive[58], lymphatic[59] or gastrointestinal systems[60]. Collagen and lipids are major PAI biomarkers in the NIR-II spectral range, enabling lipid-plaque monitoring in arterial-related diseases[61].

PAI systems for clinical applications

PAI has demonstrated promising preclinical efficacy in small animal imaging, and research has been expanding from small-scale pilot studies in humans to large-scale studies with clinical impacts; in addition, several forms of commercial PAI equipment have been launched[62–69]. Many implementations of PAI exist[70], but we describe three main forms that can be used for clinical studies, depending on the region of interest (ROI) and clinical purpose: dual-modal handheld photoacoustic and USI (PAUSI), station-based tomographic PAI, and mesoscopic and microscopic PAI.

Dual-modal PAUSI

A dual-modal PAUSI system typically adapts a traditional USI system combined with a portable pulsed laser source. The operation of this integrated PAUSI system is very similar to that of the traditional USI system, so it should be familiar to medical professionals. The integrated system can simultaneously acquire photoacoustic and ultrasound (PAUS) images of biological tissues that provide complementary information about their acoustic properties (for example, organ structures and blood flow) and optical absorption spectra (for example, Hb concentration, oxygen saturation of haemoglobin (sO_2) and the pharmacokinetics of molecular agents)[71]. The dual-modal PAUSI system can be implemented as either a handheld or endoscopic device (Fig. 2a). The handheld system uses USTRs configured as a linear array[15], phased array[72] or curvilinear array[73], together with laser fibre bundles. The primary diagnostic sites for the handheld system include the skin[40], thyroid[74], breasts[75] and limbs[76]. One advantage is that information from conventional USI analyses (for example, organ shape, size and stiffness) can incorporate information from supplementary photoacoustic analyses (for example, vascular network, angiogenesis, oxygenation and metabolism) to improve clinical outcomes[76,77]. In endoscopic implementation, endocavity USTRs, such as a transrectal array or transvaginal array, along with miniaturized laser fibre bundles[78,79], are typically inserted and used for diagnoses in internal organs. PAUS endoscopic imaging also uses the findings of complementary PAI analyses provided with the conventional USI analyses to comprehensively diagnose vaginal and rectal diseases in a wide trapezoidal field of view.

Station-based tomographic PAI

Photoacoustic waves generated inside the human body by laser irradiation generally propagate omnidirectionally. Thus, hemispherical-array[80] and/or ring-shaped-array[81] USTRs, which have larger detection apertures than linear arrays or curved arrays, are particularly well suited for detecting omnidirectional photoacoustic waves and can greatly improve the quality of photoacoustic images. These USTR geometries are typically found in station-based tomographic PAI systems (Fig. 2b). In a human experimental setup, the USTR is typically positioned beneath the imaging table and integrated with an ultrasound data acquisition device and a pulsed laser source[62]. A motorized stage moves the USTR to obtain large ROI photoacoustic images, enhancing the clinical applicability and diagnostic potential of the system[57]. Most advantageously, station-based tomographic PAI provides a deep penetration depth in humans (<5 cm)[82]. The major diagnostic target regions of this type of PAI system include the brain[83], breast[84] and limb[62].

Mesoscopic and microscopic PAI

Mesoscopic and microscopic PAI is implemented in combination with high-frequency single-element USTR under dark-field diffusive or loosely focused optical illumination. High-frequency single-element

USTRs form spherical foci with high acoustic numerical apertures and can acquire photoacoustic images with spatial resolutions of tens of microns, which is difficult to achieve with typical array-type USTRs. The mesoscopic and microscopic PAI system is held by an articulated arm for flexible positioning on the ROI and obtains 3D photoacoustic images through point-by-point raster scanning via a motorized scanner. Mesoscopic and microscopic PAI is particularly effective in diagnosing skin diseases such as skin cancer[85] or psoriasis[86,87].

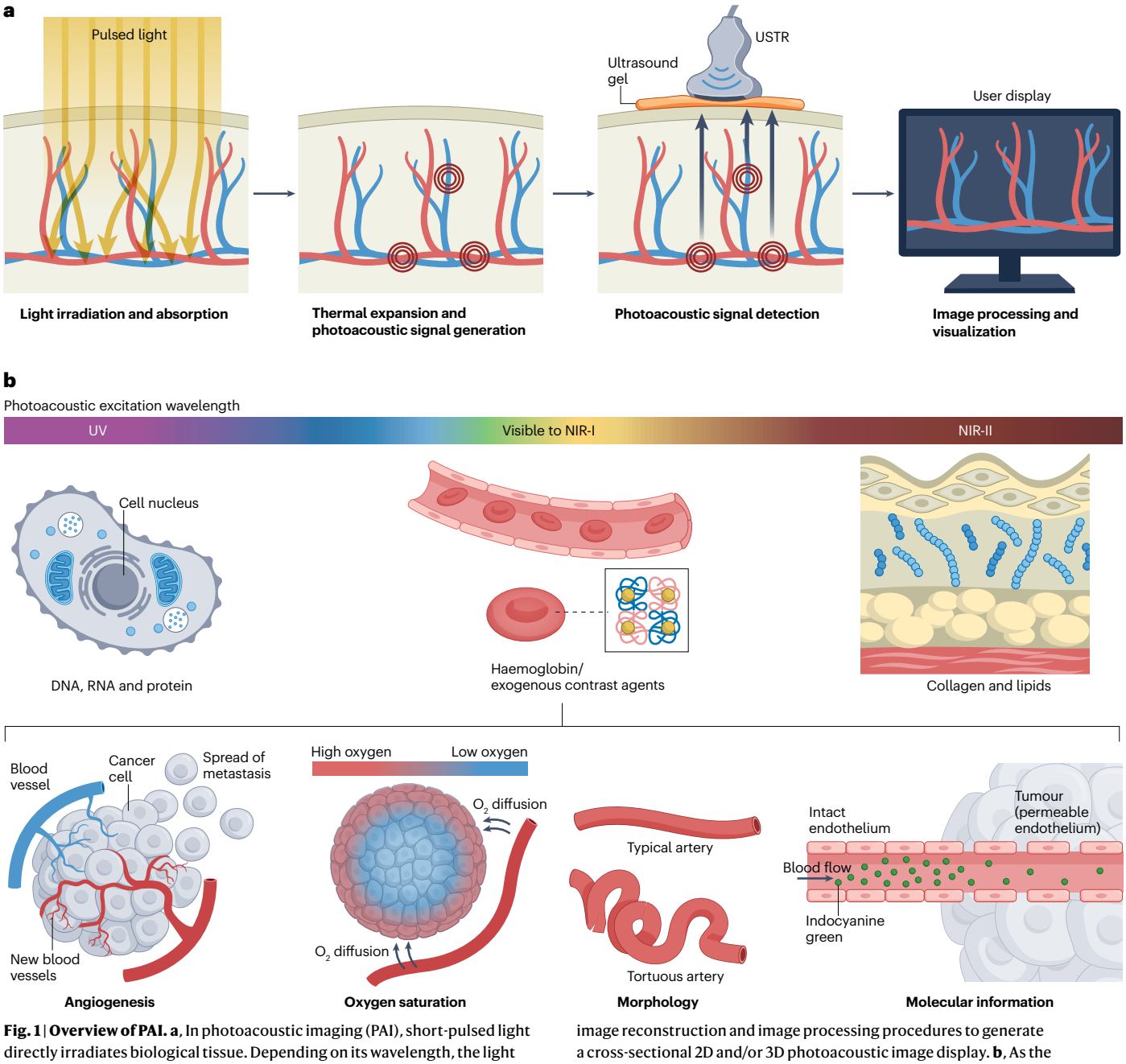

Fig. 1 | Overview of PAI. a, In photoacoustic imaging (PAI), short-pulsed light directly irradiates biological tissue. Depending on its wavelength, the light is absorbed to varying degrees by endogenous chromophores (for example, DNA, RNA, haemoglobin, melanin, collagen and lipids) or by FDA-approved exogenous contrast agents (for example, indocyanine green and methylene blue). Absorption of each light pulse results in a rapid localized temperature increase, which leads to thermal expansion and generation of an ultrasound wave (photoacoustic wave). Photoacoustic waves convey information about the optical absorption properties of the tissue. An ultrasound transducer (USTR) detects the photoacoustic signals, which undergo signal processing, image reconstruction and image processing procedures to generate a cross-sectional 2D and/or 3D photoacoustic image display. **b**, As the optical absorption coefficient of each target is wavelength dependent, the photoacoustic contrast is spectrally determined by the excitation light. PAI in the ultraviolet (UV) region can be used to image DNA, RNA and proteins, for example. PAI in the visible to near-infrared I (NIR-I) wavelength can image exogenous contrast agents and haemoglobin and can therefore be used to provide information on angiogenesis, blood oxygenation saturation, vascular morphology and molecular concentration. PAI in the NIR-II wavelength can be used to visualize collagen and lipids.

Pilot and clinical studies

In this Review, we consider pilot and clinical studies of PAI in patients with specific diseases (Supplementary Table 1). Exploratory studies with healthy volunteers or ex vivo tissues are excluded. We define a clinical study as a study that establishes the number of individuals in the study design through power and alpha values to achieve clinical significance. Studies with large numbers of patients and healthy volunteers are also classified as clinical studies if they have notable clinical findings (for example, improved diagnostic sensitivity or improved diagnostic specificity). Otherwise, the approaches are considered pilot studies. Further potential clinical applications of PAI are also highlighted (Box 1).

Integumentary system

The skin is a model organ for several optical imaging modalities (for example, optical coherence tomography[88], reflectance confocal microscopy[89] and multiphoton microscopy[90]) as it covers the outside of the body and is easily penetrated by light. Optical coherence tomography is especially suited to non-contact and real-time imaging of multiple clinical problems, including burns and grafts. However, the limited optical penetration depth of these optical modalities cannot provide information from >2 mm deep[88]. High-frequency USI is often used to monitor deeper penetration depths but its ultrasonic contrast and diagnosis specificity are limited[91]. On the other hand, PAI can readily and non-invasively obtain deeper information and volumetric skin information.

Melanoma, a cutaneous malignancy with a distinct melanin contrast, is a compelling application for PAI[92–95]. Surgical intervention remains the primary treatment to mitigate or eliminate cancer recurrence and metastasis[96]. The Breslow depth, a parameter indicating the depth of a melanoma, helps determine the needed extent of excision. Minimizing the depth and extent of excision improves post-surgical quality of life; therefore, non-invasive determination of the Breslow depth is important. PAI can detect dermal and epidermal melanoma in vivo and can evaluate Breslow depth. In one pilot study of melanomas with Breslow depths of 0.32–8.00 mm, 3D multispectral PAI yielded a mean error of 0.36 mm when spectrally unmixed photoacoustic-determined depths were matched with histopathological depths[40] (Fig. 3a1). PAI has also measured the length, width and depth of other skin tumours (acanthotic seborrhoeic keratosis and basal cell carcinoma)[93]. Another pilot study using mesoscopic PAI demonstrated differences in various vessel biomarkers between malignant melanoma and benign nevi: total blood volume (malignant 5.94% versus benign 23.62%), vessel density (0.017 arbitrary units (a.u.) versus 0.01 a.u.), average vessel length (260.39 µm versus 139.60 µm), tortuosity (0.27 a.u. versus 0.47 a.u.), fractal number (1.12 a.u. versus 1.26 a.u.) and lacunarity (0.088 a.u. versus 0.170 a.u.)[85].

Psoriasis, a chronic inflammatory skin disorder, is typically assessed using the Psoriasis Area and Severity Index[97,98]; however, it is subjective and does not evaluate subsurface characteristics in psoriatic inflammation or disease progression[99–102]. Therefore, in many cases, psoriasis diagnosis is confirmed by biopsy. Mesoscopic PAI reveals the relationship between the subsurface image features (for example, skin morphology and vascular patterns) of psoriasis and other dermatological conditions and the pathophysiological metrics of the disease[86]. Measured mean epidermal thickness in photoacoustic and histological images is strongly correlated with disease severity in patients with psoriasis. No definitive treatment exists for psoriasis but new treatments for managing the disease and suppressing symptoms have been presented. Mesoscopic PAI, with a spatial resolution of <10 µm, monitors treatment efficacy by label-free extraction of several clinical biomarkers: mean capillary loop length (MCLL), mean capillary loop diameter and mean subepidermal vascular plexus width (MPW)[87] (Fig. 3a2). These skin features are directly related to the microvasculature, which is prominently affected by inflammation, and elongation of the capillary loops is a well-known marker of psoriatic skin in histological assessment. For 19 patients receiving conventional and biologic treatments for psoriasis, PAI revealed notable improvement over the course of treatment in the biomarkers (especially MCLL and MPW) extracted from 3D images[87]. MCLL and MPW were also correlated with the Dermatology Life Quality Index in a subset of patients. Furthermore, deep learning shows the potential to segment epidermis and dermal vessels, and these findings indicate that psoriasis severity and progression can be characterized using biomarkers extracted from 3D images, including epidermis thickness, blood volume, vessel length, vessel diameter and vessel bifurcations[103]. PAI has also been used to investigate other skin diseases, including system sclerosis[104–106], Raynaud phenomenon[107], atopic dermatitis[108–112] and allergic skin reactions[113].

Musculoskeletal system

PAI has many clinical applications related to bone assessment, encompassing bone cancer, joint pathologies, spinal disorders, osteoporosis and surgical guidance for bone-related procedures[114]. PAI can characterize bone through temperature measurement, spectral parameters, guided wave analysis and spectroscopy[115–118]. It is especially effective in visualizing and identifying anatomical features such as the proximal interphalangeal joint, the distal interphalangeal joint, the phalanges and tendons[119–127].

Rheumatoid arthritis can be diagnosed with X-rays, MRI and USI. X-rays can confirm structural changes in joints, showing inflammation, damage to joint cartilage and bone, or changes in joint spaces. MRI provides detailed images of joints and surrounding tissues to determine the degree and location of inflammation. USI does not accurately provide detailed bone and joint information as provided by X-rays or MRI but is gaining importance in rheumatoid arthritis evaluation owing to its low cost and ease of use. Nevertheless, additional clinical features are needed to improve the accuracy of rheumatoid arthritis assessment by USI. Synovial hypoxia is a hallmark of the inflammatory response in rheumatoid arthritis[128]. One clinical study classified 118 patients with rheumatoid arthritis and 15 healthy volunteers into hyperoxic, intermediate and hypoxic groups (NCT04297475)[129]. Among participants with rheumatoid arthritis, the wrist synovium was categorized as being hyperoxic in 36 individuals, of intermediate oxygenation in 48 individuals and hypoxic in 34 individuals. By contrast, all 15 healthy controls had hyperoxic synovial tissues. In participants with rheumatoid arthritis, those with hypoxic synovium exhibited higher mean disease activity scores than individuals with intermediate oxygenation, including the 28-joint Disease Activity Score (5.3 a.u. versus 3.6 a.u.) and the Clinical Disease Activity Index (26.0 a.u. versus 11.0 a.u.).

PAI provides excellent images of soft tissue in the immediate vicinity of bones and joints, especially muscles and could therefore be useful for characterizing muscle tissue in neuromuscular disease. PAI has already been shown to visualize the fibro-fatty degeneration of muscle tissue in primary and congenital diseases such as Duchenne muscular dystrophy (DMD) (NCT03490214)[44]. DMD is the predominant lethally inherited X-chromosomal muscular disease, characterized by cascades of inflammation and subsequent fatty and fibrotic transformations. MRI has shown potential as a non-invasive imaging modality

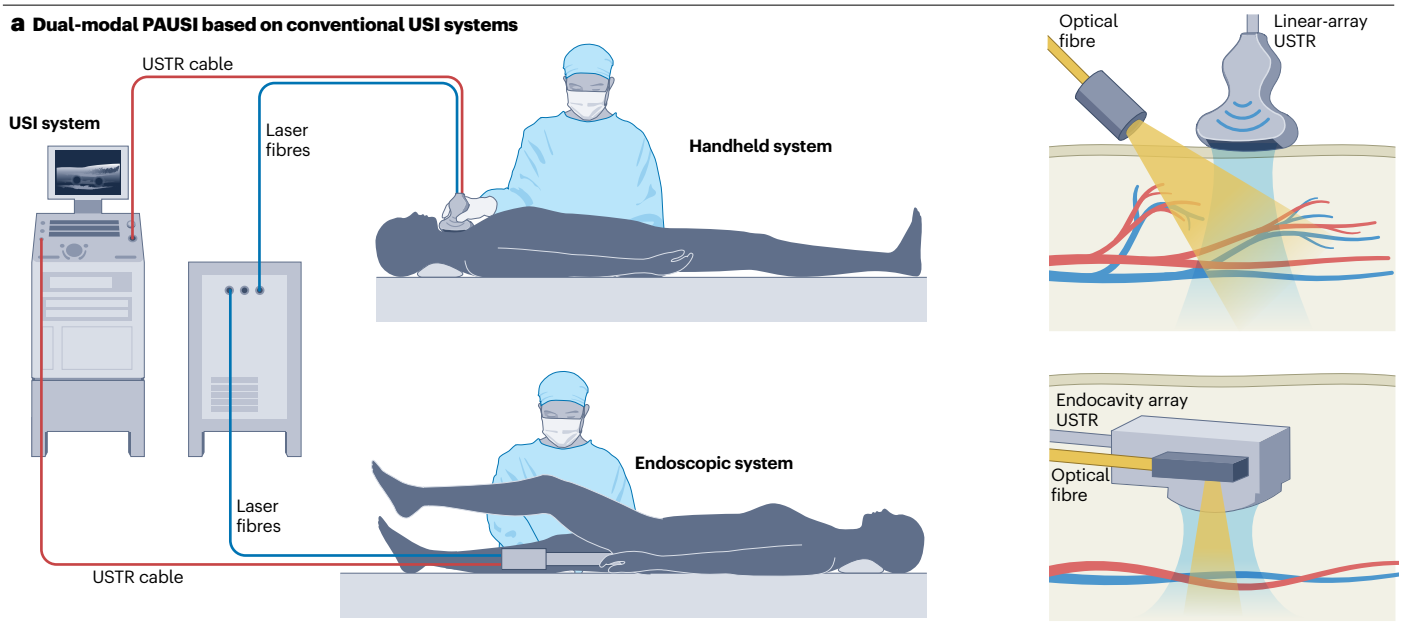
a Dual-modal PAUSI based on conventional USI systems
USTR cable
USI system
Laser fibres
Handheld system
Endoscopic system
Laser fibres
USTR cable
Optical fibre
Linear-array USTR
Endocavity array USTR
Optical fibre

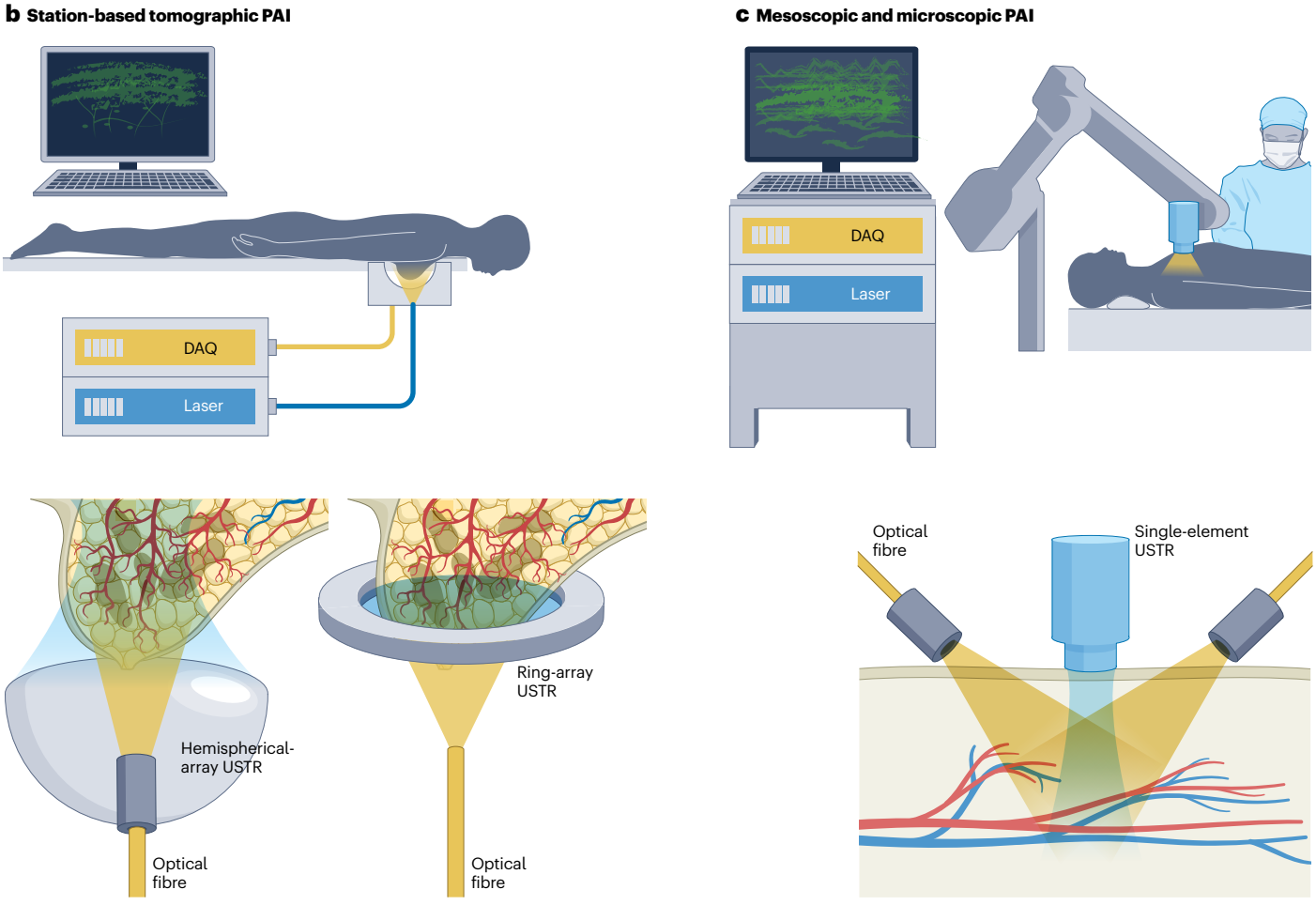
b Station-based tomographic PAI
DAQ
Laser
c Mesoscopic and microscopic PAI
DAQ
Laser
Hemispherical-array USTR
Optical fibre
Ring-array USTR
Optical fibre
Optical fibre
Single-element USTR

Fig. 2 | Various clinical PAI system configurations. a, Dual-modal photoacoustic and ultrasound imaging (PAUSI), based on conventional ultrasound imaging (USI) systems, can be categorized into a handheld type with linear-array ultrasound transducers (USTRs) and an endoscopic-type with endocavity array USTRs. Primary diagnostic sites for the handheld-type system include the skin, thyroid, breast and limbs; diagnostic sites for the endoscopic-type system include the stomach, vaginal and rectal regions. **b**, Station-based tomographic photoacoustic imaging (PAI) using hemispherical-array USTRs or ring-array USTRs. The primary diagnostic sites for station-based tomographic PAI include brain, breast and limb. **c**, Mesoscopic and microscopic PAI using a high-frequency single-element USTR. The primary diagnostic site for mesoscopic and microscopic PAI includes skin. DAQ, data acquisition.

for quantifying disease pathology and progression in DMD, but its long acquisition time is not suitable for young children. In addition, in the context of fibrosis detection, MRI is limited by the non-specific nature of signal alterations in T2-weighted, water-sensitive MRI images[44]. However, 2D PAI showed noteworthy differences in the mean collagen values of patients with DMD and those of healthy volunteers (24.7 a.u. versus 14.6 a.u.) but no significant differences between the two groups in lipid content, HbO_2, HbR and total Hb (HbT). 3D PAI also showed a significant difference in mean collagen value between patients with DMD and healthy volunteers (11.4 a.u. versus 5.4 a.u.) and also showed significant differences between groups in HbO_2, HbR and HbT (Fig. 3b).

Cardiovascular system

Cardiovascular disease includes conditions such as peripheral arterial disease, ischaemic heart disease, hypertension, cardiomyopathy, valve disease, arrhythmia and stroke[130]. The examination of microcirculation is crucial in the assessment of peripheral vascular conditions, especially diabetic foot problems. However, conventional ultrasound Doppler imaging focuses on major arteries, limiting its ability to offer microvascular insights in the early stages of cardiovascular disease. Furthermore, the cost of both magnetic resonance angiography and X-ray CT angiography limits their frequent use for prognosis monitoring. One clinical study involving 197 participants suggested that photoacoustic-derived HbO_2 is a strong biomarker for determining the three clinical stages of peripheral arterial disease: healthy volunteer, intermittent claudication at any walking distance (Fontaine II), and critical limb-threatening ischaemia with resting pain, ulcer or gangrene (Fontaine III/IV) (NCT04641091)[131]. Furthermore, the categorization of ankle-brachial index (ABI) measurements into four groups showed that HbO_2 levels decreased with decreasing ABI values. In a subgroup of 58 patients with critical limb-threatening ischaemia, ABI values were classified as plausible (<0.74) or implausible (0.75–1.3 or media sclerosis >1.3) based on their alignment with clinical stages and angiographic findings. HbO_2 decreased from the plausible to implausible groups, indicating that PAI detected clinical stage more precisely in this subgroup.

Another pilot study involving 12 patients with arteriovenous or venous vascular malformations demonstrated that PAI revealed notable distinctions between various types of vascular malformations in terms of the ratio of HbO_2 to HbR[132]. Additionally, PAI facilitated the quantitative evaluation of therapeutic responses following procedures such as embolization or sclerotherapy.

Several PAI implementations have been used to visualize carotid artery plaques to assess the risk of ischaemic stroke[133,134]. As multispectral PAI can resolve lipids and Hb, it can reveal plaque in the arterial lumen of patients with carotid atherosclerosis. Multispectral PAI was shown to distinguish differing fat-to-blood ratios between patients and healthy volunteers ($P = 0.001$) and between plaque and lumen in patients ($P = 0.04$)[135] (Fig. 3c).

Prompt diagnosis of severe anaemia, a life-threatening condition encountered in various medical disciplines, is imperative for optimizing patient outcomes, but few dependable, non-invasive, point-of-care diagnostic tools exist at present. In a pilot study, PAI demonstrated exceptional efficacy in identifying patients with severe anaemia, relying on a robust positive correlation between the photoacoustic-derived HbR value and photoacoustic signals at 700 nm, concomitant with absolute Hb concentration[136].

Lymphatic system

Accurate visualization of lymphatic vessels is vital in diagnosing and monitoring lymphatic diseases as well as in preoperative planning for lymphoedema surgery and its postoperative evaluation. One pilot study used ICG to obtain 3D images of both lymphatic vessels and adjacent venules[59] (Fig. 3d1). Unlike visualization of blood vessels, the visualization of lymphatic vessels, devoid of inherent pigmentation, can be facilitated by a contrast agent such as ICG. Images of the lower limbs were acquired using both PAI and NIR fluorescence (NIRF) imaging in 15 participants, including a woman with a history of gynaecological cancer treated with hysterectomy, lymph node dissection and chemotherapy. PAI provided a more detailed 3D representation of the lymphatic vessels than did NIRF imaging, offering improved understanding of the spatial

Box 1 | Potential clinical applications of photoacoustic imaging

Photoacoustic histopathology

Microscopic photoacoustic histopathology can be implemented with ultraviolet light, capitalizing on the strong photoacoustic signals generated from DNA and RNA. Unlike conventional optical microscopy, a photoacoustic histopathology system can observe cell membranes, cell nuclei and intracellular materials at micro or sub-micron scale without chemical staining (for example, haematoxylin & eosin staining)[245]. This innovative approach can potentially enable pathologists to promptly assess disease status, including intraoperatively, by circumventing the labour-intensive processes of tissue freezing, fixation and sectioning required for conventional chemical staining methods. While the seamless integration of conventional intraoperative histopathology is challenging, the efficacy of photoacoustic histopathology is being substantiated through the examination of specimens from human patients with diseases such as bone cancer[242], breast cancer[246], colon cancer[42] and liver cancer[42].

Radiation-induced acoustic imaging

Radiation-induced acoustic imaging, a novel technique in radiotherapy, utilizes the acoustic waves generated by the interaction of ionizing radiation with tissues. This method can uniquely monitor and quantify the 3D radiation dose distribution during cancer treatments, offering real-time, adaptive feedback that can potentially improve treatment efficacy[247].

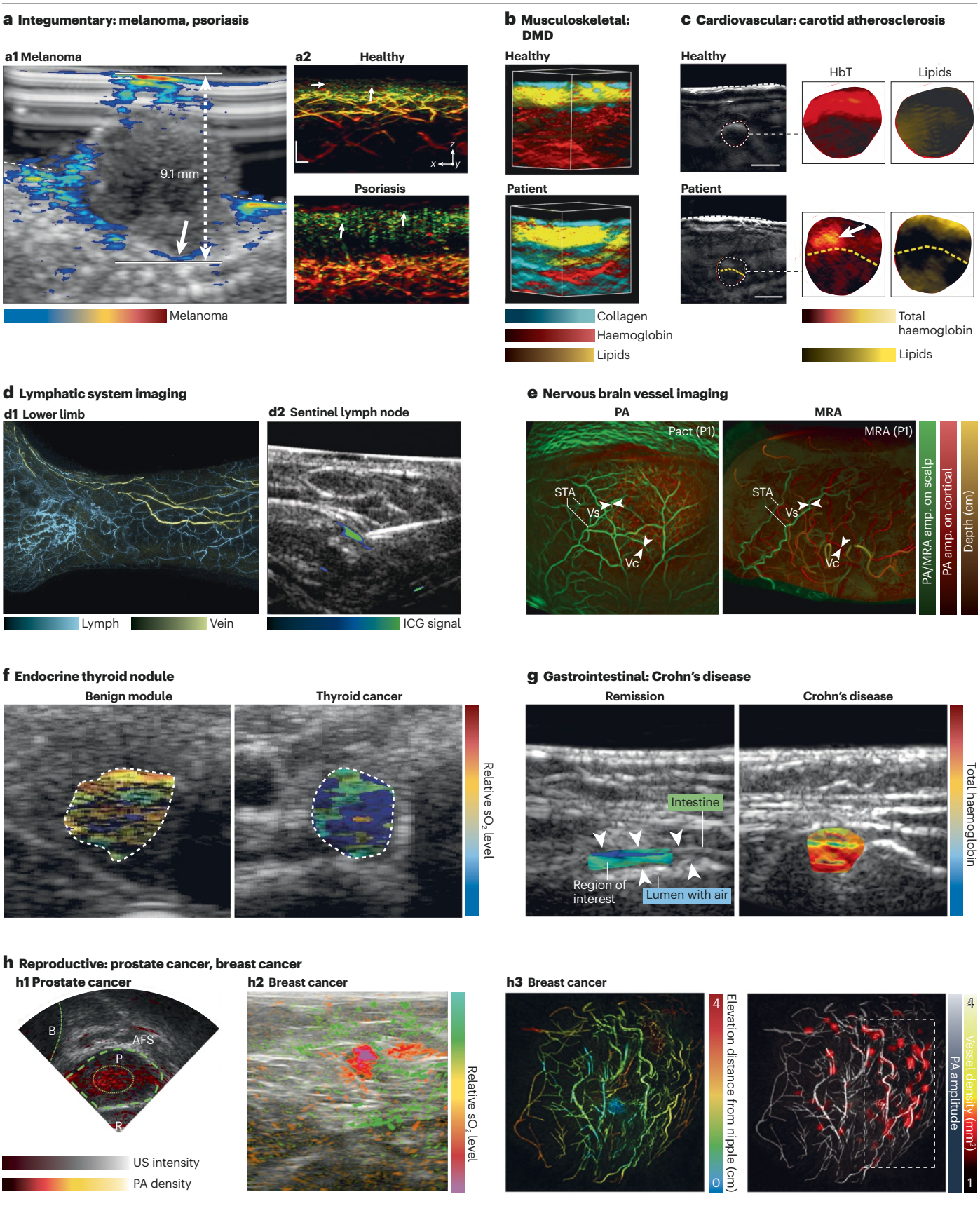
a Integumentary: melanoma, psoriasis
a1 Melanoma
9.1 mm
Melanoma
a2
Healthy
Psoriasis
b Musculoskeletal: DMD
Healthy
Patient
Collagen
Haemoglobin
Lipids
c Cardiovascular: carotid atherosclerosis
Healthy
HbT
Lipids
Patient
Total haemoglobin
Lipids
d Lymphatic system imaging
d1 Lower limb
Lymph
Vein
d2 Sentinel lymph node
ICG signal
e Nervous brain vessel imaging
PA
MRA
Pact (P1)
MRA (P1)
STA
Vs
Vc
PA/MRA amp. on scalp
PA amp. on cortical
Depth (cm)
f Endocrine thyroid nodule
Benign module
Thyroid cancer
Relative sO2 level
g Gastrointestinal: Crohn's disease
Remission
Crohn's disease
Intestine
Region of interest
Lumen with air
Total haemoglobin
h Reproductive: prostate cancer, breast cancer
h1 Prostate cancer
B
AFS
P
R
US intensity
PA density
h2 Breast cancer
Relative sO2 level
h3 Breast cancer
4
Elevation distance from nipple (cm)
0
PA amplitude
Vessel density (mm2)
4
1

Fig. 3 | Representative clinical photoacoustic imaging results for human functional systems. a, Integumentary system. **a1**, Photoacoustic and ultrasound (PAUS) image of a melanoma[40]. **a2**, Photoacoustic (PA) images of a healthy volunteer and a patient with psoriasis[87]. **b**, Musculoskeletal system: 3D PA images of a healthy volunteer and a patient with Duchenne muscular dystrophy (DMD)[44]. **c**, Cardiovascular system: PAUS images of a healthy volunteer and a patient with carotid atherosclerosis[135]. The arrow points to the region of increased total haemoglobin (HbT). **d**, Lymphatic system. **d1**, PA image of the lower limb of a 75-year-old woman with secondary lymphoedema[244]. **d2**, PAUS image of a sentinel lymph node after indocyanine green (ICG) injection[141]. **e,** Nervous system: 3D maximum amplitude projection PA and magnetic resonance angiography (MRA) images of a volunteer after post-hemicraniectomy[83]. **f**, Endocrine system: PAUS images of a benign nodule and papillary thyroid cancer[47]. **g**, Gastrointestinal system: PAUS images of Crohn's disease in remission and active Crohn's disease (both according to Simplified Endoscopic Score for Crohn's Disease)[148]. Arrows point to the large bowel and small intestine. **h**, Reproductive system. **h1**, PAUS image of prostate cancer[79]. **h2**, PAUS image of a breast tumour provided by an FDA-approved PAUS imaging system[77]. **h3**, 3D maximum amplitude projection PA images of a breast tumour[81]. AFS, anterior fibromuscular stroma; B, bladder; P, prostate; R, rectum; sO_2, oxygen saturation of haemoglobin; STA, superficial temporal arteries; US, ultrasound; Vc, cortical vessel; Vs, scalp vessel. Part **a1** reprinted with permission from ref. 40, Wiley. Part **a2** reprinted with permission from ref. 87, AAAS. Part **b** reprinted from ref. 44, Springer Nature Limited. Part **c** reprinted with permission from ref. 135, Elsevier. Part **d1** reprinted with permission from ref. 244, Elsevier. Part **d2** reprinted with permission from ref. 141, JAMA. Part **e** reprinted from ref. 83, Springer Nature Limited. Part **f** reprinted with permission from ref. 47, AACR. Part **g** reprinted with permission from ref. 148, *New England Journal of Medicine*. Part **h1** reprinted with permission from ref. 79, AAAS. Part **h2** reprinted with permission from ref. 77, Elsevier. Part **h3** reprinted from ref. 81, Springer Nature Limited.

relationship between lymphatic vessels and surrounding venules. By using multiple wavelengths, PAI could also differentiate individual lymphatic vessels from blood vessels, which are barely discernible on NIRF images, and visualized more lymphatic vessels than NIRF[59]. In two pilot studies involving patients with lymphoedema, PAI utilizing ICG successfully identified lymphatic vessels and veins in various regions and visualized their position and contractility[137,138].

Lymph nodes are important in predicting the degree of cancer metastasis and setting treatment directions[139]. The metastatic condition of sentinel lymph nodes (SLNs) is the most pertinent prognostic factor in various cancers, including breast cancer and melanoma. Lymphoscintigraphic imaging with technetium (Tc^{99m}) is the conventional method of SLN detection but this imaging technique has poor spatial resolution, presents logistical challenges, and raises radiation concerns for patients and medical staff. Two clinical trials showed the promise of using multispectral PAI to determine the metastatic status of SLNs[140,141]; in one of these trials, 165 SLNs were excised from 83 patients, and the concordance rate between SLN detection using ICG-labelled PAI and Tc^{99m}-marked methods was 94.6% (n = 106 of 112)[142] (Fig. 3d2). Intraoperatively, PAI with the addition of a NIR camera identified 159 SLNs, and a γ-probe identified 165 SLNs, resulting in a concordance rate of 96.4%. PAI visualized the SLNs in most anatomic regions, achieving a notable penetration depth of 5 cm.

Nervous system

Spinal muscular atrophy, a neuromuscular genetic disease in which muscles gradually atrophy from damage to or loss of motor neuron genes in the spinal cord and brainstem, can be characterized by PAI (NCT04115475)[142,143]. Photoacoustic signals at 800 nm showed a notable distinction between 10 individuals with spinal muscular atrophy and 10 healthy volunteers (54.0 a.u. versus 58.6 a.u.), exhibiting a more robust correlation than conventional assessments such as the Hammersmith Functional Motor Scale Expanded and the Revised Upper Limb Module.

The brain, the central hub of the nervous system, regulates complex physiological and cognitive processes and is essential to the overall functioning and integration of the nervous system. While blood-oxygen-level-dependent (BOLD) functional MRI (fMRI) represents brain activity intensity in relative terms rather than providing a quantitative measurement of brain activity, PAI offers a direct sensitivity to both HbO_2 and HbR, enabling the provision of quantitative values for brain sO_2. The linear relationship between their distinctive spectral signatures enables the quantification of sO_2 and cerebral blood volume. PAI shows remarkable brain vessel images, comparable with those from magnetic resonance angiography (Fig. 3e). A comparison of functional PAI and BOLD fMRI images from four patients who had had a hemicraniectomy revealed a robust spatial alignment within the same field of view and a substantial temporal correlation between photoacoustic and BOLD signals[83]. Importantly, the implementation of PAI enables identification of functional activation with better temporal resolution than is achievable with fMRI. Nevertheless, acoustic reverberation attributed to the presence of the skull introduces challenges to image quality, and PAI of the human brain could be constrained unless an incision is made.

Endocrine system

Imaging the endocrine system can provide clinical insights into the structure, function and pathology of the endocrine glands. Imaging aids the detection, localization and monitoring of abnormalities, guides treatment decisions, and facilitates minimally invasive interventions by providing precise lesion targeting[144]. As an example, to identify malignant thyroid nodules, the shape and size of thyroid nodules are evaluated using USI, and a biopsy is performed to determine whether the cells are malignant. In a clinical study of 52 patients, PAI of thyroid nodules classified cases of papillary thyroid cancer (PTC) and benign nodules (NCT04248166)[47] (Fig. 3f). The sO_2 level and the skew angle in the sO_2 distribution in the nodule area, together with multiparametric photoacoustic analysis using support vector machines, enabled the classification of PTC nodules. By combining the photoacoustically indicated probability of PTC with the American Thyroid Association Guidelines, the ATAP scoring method was developed, achieving a sensitivity of 100% and a specificity of 55% (a threefold higher specificity than conventional American Thyroid Association Guidelines). The sensitivity and specificity of the ATAP scoring method are comparable to those of existing ultrasound elastography, indicating that PTC screening could be combined with multispectral PAI and ultrasound elastography and show synergistic benefits. Furthermore, overdiagnosis from fine needle aspiration, the standard treatment for diagnosing thyroid cancer, could be reduced.

Another pilot study used multispectral PAI to characterize benign and malignant thyroid disorders in 18 patients[145]. HbR and HbT PAI values were significantly higher in patients with Graves disease than in control tissues (HbR: 3.18 a.u. versus 2.13 a.u.; HbT: 8.34 a.u. versus 6.59 a.u.), while the fat content values were lower in patients with Graves disease than in control tissues (0.64 a.u. versus 1.69 a.u.). In addition, malignant thyroid nodules exhibited notably lower sO_2

(55.4% versus 60.8%) and lower fat content (0.62 a.u. versus 1.46 a.u.) than did benign nodules.

Diabetes mellitus is a complex metabolic disorder with a rising global incidence. Diabetes mellitus affects both the macrovasculature and microvasculature across multiple organs, encompassing the heart, brain, lower limbs, retinas, peripheral nerves, kidneys and skin. Attempts are being made to use PAI to diagnose and monitor the progress of diabetes by measuring peripheral vascular changes and/or microvascular changes in the skin. One clinical study involving 103 patients with diabetes and 48 healthy volunteers determined diabetes status from six photoacoustic biomarkers of the skin: small vessel number (3.45 a.u. in patients with diabetes versus 9.78 a.u. in healthy volunteers), large vessel number (13.39 a.u. versus 20.34 a.u.), total vessel number (16.87 a.u. versus 30.12 a.u.), total blood volume (1.58% versus 4.21%) and epidermal thickness (105.27 μm versus 81.03 μm)[146]. These five biomarkers were also significant in patients with diabetic neuropathy and atherosclerosis, indicating the clinical scalability of this method. Another study used deep learning to identify the 32 most relevant photoacoustic dermal features of diabetes and predict the presence of diabetes through a microangiopathy score[147].

Gastrointestinal system

Crohn's disease is a chronic inflammatory bowel disorder that affects the entire gastrointestinal tract. Besides clinical parameters, reference standard imaging modalities to assess inflammation include endoscopy with subsequent biopsy sampling, CT enterography (CTE), and magnetic resonance enterography (MRE). Endoscopy is invasive, time-consuming, has the potential for complications and is not suitable for frequent monitoring. CTE and MRE are commonly used non-invasive methods but involve drinking 1 l of liquid with an oral contrast agent. CTE provides quick results but exposes the patient to ionizing radiation; MRE is radiation-free but requires a longer examination time and additional use of antiperistalsis agents. By contrast, PAI can rapidly and non-invasively determine the presence of inflammatory activity in Crohn's disease. In a clinical study of 108 patients, a transabdominal PAI system evaluated the degree of intestinal inflammation (NCT02622139)[148] (Fig. 3g). The distributions of multispectral photoacoustic analyses were compared between patients with active Crohn's disease and those with non-active disease, alongside other clinical measures, including clinical scoring (Harvey–Bradshaw index), endoscopic scoring (Simplified Endoscopic Score for Crohn's Disease) and histological scoring (modified Riley score). Using endoscopic scoring as the reference standard, photoacoustic signals at 900 nm exhibited the highest sensitivity (100.0%) and specificity (77.8%), with an AUC of 0.92. HbT showed a sensitivity of 100.0%, a specificity of 77.8% and an AUC of 0.91. Comparatively, other assessments, such as the Harvey–Bradshaw index (AUC 0.57), C-reactive protein (AUC 0.79) or ultrasound Limberg score (AUC 0.77), demonstrated lower diagnostic performance levels. Similar trends were observed in histological comparisons of the different groups. Based on these results, PAI-derived measurement of Hb levels in the intestinal wall holds potential as a non-invasive procedure for differentiating between active disease and remission in patients with Crohn's disease, potentially reducing invasive procedures.

The same group also studied 44 patients with ulcerative colitis, a chronic inflammatory condition of the gastrointestinal tract requiring lifelong clinical and endoscopic reassessment of inflammatory activity (NCT02622139)[149]. Patients with endoscopically and clinically confirmed active ulcerative colitis demonstrated significantly higher photoacoustic signals than patients in a state of remission at 760 nm (60.53 a.u. versus 49.74 a.u.) and 800 nm (54.57 a.u. versus 45.87 a.u.). Multispectral photoacoustic values, such as HbR and HbT, also showed stronger signal levels in patients with active ulcerative colitis. The Riley score was 4.22 in patients in remission versus 8.56 in patients with active ulcerative colitis. In short, PAI can diagnose disease activity in ulcerative colitis by quantitative assessment using multispectral analysis. Patients with chronic intestinal inflammation often have low food intake and low body weight, making them a suitable patient group for PAI assessments. PAI is not always realistically feasible in patients with a higher body weight and thus a higher required penetration depth, and the errors can increase. PAI might therefore also be useful in children and young people, and a study with 23 paediatric patients with inflammatory bowel disease also showed increased Hb signals in inflamed areas of the intestine[150].

A multicentre study (NCT04456400) aims to confirm these first encouraging results. Final results have not yet been published; however, the data may not provide such clear trends. To replace endoscopy, a high degree of certainty in detecting even minor inflammatory activity is needed. Development of a clinical-grade imaging system that provides sufficient stability across the heterogeneity of different centres and users is challenging.

Reproductive system

Transrectal ultrasound (TRUS)-guided prostate biopsy is a standard method that sometimes results in under-detection or over-detection of cancers; elastography or angiography are needed to classify cancers as malignant or benign and to improve sensitivity and specificity. MRI-guided TRUS fusion biopsy and molecular imaging, such as hyperpolarized ^{13}C MRI and PET, provide more accurate biopsies and better assessment of the prognosis for treatment than TRUS-guided biopsy alone. However, MRI and PET are limited by their requirement of frequent screening or real-time biopsy. Alternatively, integration of an endoscopic PAI system with TRUS to guide prostate biopsy has been proposed[79]. In a pilot study, a transrectal USTR, combined with a laser fibre, captured simultaneous transrectal PAUS images from 20 patients with prostate cancer. Transrectal PAUSI successfully identified malignant prostate regions using anatomical ultrasound images and Hb-based or ICG-based photoacoustic images[79]. Label-free PAI visualized the vascular distribution in the prostate and surrounding tissues, while ICG-aided PAI provided contrast-enhanced photoacoustic images within the prostate. Multiwavelength PAUS results were confirmed by simultaneous PET–MRI and subsequent targeted biopsy results, suggesting that transrectal PAUS might compensate for the shortcomings of PET–MRI. Despite the small number of patients, this study demonstrated the ability of an endoscopic PAI system to identify prostate cancers (Fig. 3h1). Another approach integrated the optical components of a photoacoustic sensing probe directly into a needle, and showed that it might be possible to distinguish between healthy and diseased prostate tissue[151]. Further study would need to show the additional benefit of PAI in minimizing false negative findings and show that it does not lead to overtreatment in this population. The lack of tailored PAUSI studies for the prostate to date is due to the relatively high invasiveness of the technique and higher regulatory requirements compared with other transabdominal imaging approaches. The incentive for companies to invest in this very specific, narrow application – with many competing ultrasound modalities – might not be high enough at present owing to the sparse data available.

Breast imaging is one of the most prominent PAI research topics, possibly partly because breast tissue has good properties for optical imaging[152]. Although the first advances occurred more than 25 years ago, the technique has disappointingly not yet become established in routine practice. The main application for PAI was initially sought in a screening setting, especially because conventional imaging modalities, such as X-ray mammography and USI, can lack optimal sensitivity and specificity[153]. A clinical study of 1,690 patients with 1,757 masses demonstrated that PAUSI, a potentially superior clinical alternative, can help diagnose cancer with high sensitivity (96%) and specificity (43%), resulting in a 14.9% increase in sensitivity and 2.6% decrease in specificity compared to grey-scale USI alone. PAUS images in breast cancer produce grey-scale ultrasound images of breast morphology, while photoacoustic functional parameters of HbT and sO_2 highlight the tumour[75] (Fig. 3h2). Co-registered functional and anatomical 2D PAUS images can increase the accuracy of the radiological assessment of malignancy scored according to the Breast Imaging Reporting And Data System (BI-RADS). The negative likelihood ratio of 0.094 for the PAUS images indicates that a negative examination can reduce a maximum ultrasound-assigned pretest probability of 17.8% (low BI-RADS 4B) to a post-test probability of 2% (BI-RADS 3). PAUSI has thus demonstrated its ability to reduce the number of false-positive examinations and biopsies of benign masses in breast imaging.

In addition to the dual-modality PAUSI system, a station-based PAI system specific to breast cancer has been developed[81,154,155]. This station-based PAI system using a photoacoustic-optimized USTR provides a detailed 3D photoacoustic image of the angiographic structures of tumours with high spatiotemporal resolution and superior penetration depth (~4 cm) (Fig. 3h3). One pilot study used blood vessel densities quantified by photoacoustic images to identify breast tumours from eight patients using receiver operating characteristic curves (average sensitivity 87% and specificity 85.9%). The mean of the average vessel density ratios of the six malignant tumours was 1.4 times higher than that of the two benign tumours[81]. These results suggest that diagnosis by non-ionizing PAI has advantages over conventional mammography, providing better sensitivity in radiation-dense breasts while being more readily clinically available. Unlike mammography, PAI does not require compression of the patient's breast. In addition, unlike MRI, PAI maps Hb contrast without labels, so information similar to that provided by contrast-enhanced MRI can be obtained at higher spatial resolution and faster imaging speeds — attributes that are advantageous for frequent monitoring.

To demonstrate superiority in a high-throughput application, such as a population-wide screening programme, enormous study populations and investments are required. Whether PAI is sensitive enough to detect vascular changes in the early stages of tumour development must be questioned as should whether detection of neoangiogenesis is a proper biomarker or biological process for a screening scenario. In addition to the pure proliferation of tumour cells, genetic changes and other subcellular processes play a role early in tumour evolution[156] and currently elude detection by PAI.

More than half a dozen different imaging systems exist in the context of PAI breast imaging[65,77,81,157–161], but very few have developed into a commercial system available on the market. The heterogeneity of the developed PAI technologies and the data produced means that cross-platform comparisons cannot currently be made. Comparing these data in meta-analyses will be necessary to provide further evidence for widespread clinical use.

Challenges of clinical translation

The ability of PAI to probe diverse symptomatic manifestations in deep tissue suggests novel avenues in precision medicine. To overcome the obstacles impeding its clinical application, such as low trial approval rates in clinical trials and the lack of high-impact, transformative findings, studies that have encountered limitations should be reassessed. For example, a study showing how PAI could be useful in visualizing fibro-fatty degeneration of muscle tissue in DMD[44] illustrates ambiguities in PAI interpretation: the 2D and 3D photoacoustic analyses are discrepant. In another pilot study investigating the use of PAI detection of lymph node metastases in patients with oral cancer[162], ex vivo assessments indicate a marked increase in the concentrations of EGFR-targeted contrast agents in malignant cases but, in vivo, the mismatch of imaging positions between the scans before and after injection of contrast agent meant that it was difficult to delineate such differences (NCT03757507, NCT03134846). In the imaging of thyroid nodules, where PAI has demonstrated exceptional efficacy, a 2023 study[163] (NCT04730726) reported an absence of statistically significant disparities between malignant and benign nodules based on PAI multi-parameters, such as HbO_2, HbR and sO_2, in contrast to earlier findings. In this section, we discuss the root causes of the above failures, pinpointing the technical limitations inherent in PAI, and exploring the industrial and ethical challenges of integration of PAI into clinical practice.

Technical challenges

Major technical challenges in PAI arise from optical excitation and acoustic detection. Light at optical wavelengths has limited imaging depth in tissue and creates many uncertainties.

First, the maximum light penetration depth is greatly limited by strong light scattering in biological tissue. However, optical illumination with a long wavelength, averaged over multiple frames, can increase the penetration depth. For example, for the same surface irradiated with a laser fluence proportional to the maximum allowable exposure, 1,064 nm light (NIR-II) penetrates more deeply (<6 cm) than light in the range 740–800 nm (NIR-I)[164]. In addition, multi-angle illumination can improve image quality over fixed angle by improving the imaging depth, SNR and contrast-to-noise ratio[165]. Moreover, by switching wavelengths quickly (within 20 ms), fast-sweep PAUSI can acquire multiple frames of multiwavelength photoacoustic images at once in a single ultrasound image. This capability improves the SNR and imaging depth by applying real-time motion compensation and averaging across multiple frames[54].

Second, because light distribution in tissues is heterogeneous, it is difficult to satisfactorily compensate for the light fluence in tissues and achieve accurate measures of functional parameters (for example, HbO_2, HbR and sO_2). This long-standing problem has spurred studies to overcome it. For example, differences in microvessel brightness owing to optical attenuation of the tissue can be compensated for by using background-level brightness[77]. In addition, eigenspectral PAI has improved the accuracy of spectral analysis by modelling the spectral pattern of the optical fluence[166]. Monte Carlo simulation can also be employed for fluence compensation[167]. More recently, a fast-sweep beam has demonstrated real-time wavelength-dependent fluence compensation[54].

Achieving high-sensitivity acoustic detection, utilizing larger apertures and encompassing a broad bandwidth are crucial to visualizing deep tissue structures and providing valuable information about tissue properties and biomarkers. Fundamentally, PAI is highly dependent on the performance of the USTR.

PAI image quality is affected by limited-view artefacts induced by features of the USTR such as the aperture shape or arrangement, number of elements, and directional sensitivity. Limited-view artefacts are caused by the limited aperture of USTR, where only a portion of photoacoustic signals spreading omnidirectionally from the target is detected, and the complete structure of the target cannot be reconstructed back to the image, resulting in image distortion. A linear-array USTR can detect photoacoustic signals from deep tissue in only a narrow angle of view; arc-shaped, ring-shaped and hemisphere-shaped array USTRs are more effective for PAI because they can detect photoacoustic signals over a wide angle of view[36]. Linear-array USTRs are employed in various conventional USI applications but arc-shaped, ring-shaped and hemisphere-shaped array USTRs are seldom used in USI. Achieving simultaneous high-quality ultrasound and photoacoustic images in the framework of PAUSI is therefore challenging.

Piezoelectric-based USTRs, widely employed in conventional USI, have limited sensitivity and bandwidth. PAI benefits from broadband USTRs that can detect diverse frequency information. In most cases, a high-frequency component occurs in relatively thin and point-like targets such as blood vessels and a low-frequency component occurs in large targets such as organs[168,169]. However, a bandwidth-limited USTR selectively detects the photoacoustic signals based on its specifications[168], which raises the question of whether a photoacoustic signal obtained through a USTR can be representative enough to perform quantification such as spectral unmixing. As an alternative, USTRs based on micro-electromechanical systems, such as capacitive micromachined USTR (cMUT) and piezoelectric micromachined USTR, have emerged[170,171]. Relative to piezoelectric-based USTR, cMUT generally provides a broader bandwidth and piezoelectric micromachined USTR exhibits better sensitivity[172]. cMUT has been introduced as a commercial product, and research efforts are under way to explore its application in PAI[173].

The optical opacity of conventional USTRs hinders laser light delivery, even blocking light entirely. Ring-shaped USTRs have been actively applied in PAI to enable the passage of laser light, but these designs compromise acoustic sensitivity and focusing ability. To address these limitations, optically transparent USTRs have been introduced, facilitating direct passage of excitation light[174–176]. Moreover, to tackle the ongoing issue of limited sensitivity and bandwidth of USTRs, an optical sensing technology with an inherently ultra-wide frequency sensing range has been implemented. A Fabry–Pérot interferometer[177,178], a micro-ring resonator[179,180] and a Bragg grating[181,182] often surpass the frequency bandwidth of traditional piezoelectric devices, offering the potential for developing compact, transparent USTRs. Furthermore, non-contact and non-interferometric methods, such as photoacoustic remote sensing, overcome the need for physical contact with the sample to detect the signal. This non-contact technique has the potential to greatly contribute to the diversity of PAI applications, and ultraviolet wavelength-based photoacoustic histopathology has been studied[183,184]. Nonetheless, the clinical adoption of optical detection technology for PAUSI could still be constrained as conventional USI commonly relies on piezoelectric-based USTRs.

Industrial challenges

The clinical translation of PAI will require concurrent industrial translation. To achieve widespread adoption, the costs of PAI must be carefully considered. Commercial PAUSI is an expensive system affordable by only a few medical centres. A pulsed laser diode[185] and a light-emitting diode (LED)[186] have been highlighted as useful photoacoustic laser sources owing to their cost-effectiveness, compact size and high pulse-repetition frequency. Systems can also benefit from economies of scale — both laser diode-based and LED-based systems will likely benefit from developments in the semiconductor industries where manufacturing volume drives cost reduction and competition increases energy output[187,188]. Similarly, systems with higher-power lasers will benefit from economies of scale enabling volume manufacturing to drive cost reduction. As point-of-care ultrasound and ultrasound market competition increases, the cost of systems with integrated ultrasound will likely reduce[189].

Ensuring reliability and cost benefit in clinical use is key to PAI being adopted clinically. Cost–benefit information can be shown in controlled clinical trials but reliability in daily clinical use requires considerable product engineering. For example, ultrasound systems have an expected lifetime of up to 9 years and users will probably expect similar lifetimes of PAI equipment even with the added complexity of the laser equipment. Servicing optical components in the field can also be challenging owing to factors such as the sensitivity of optics to dust and contamination, exposure of the clinical environment to higher energy laser output, and the need for specialized equipment and technician training[190].

Ethical challenges

Ethical considerations for the implementation of PAI require a multidimensional perspective. Firstly, although high ethical standards might imply patient safety in the context of PAI usage, this consideration alone is not enough. In contrast to new pharmaceuticals, medical devices have different approaches to research and development, assessment of safety and effectiveness, how the innovation process is integrated into clinical practice in collaboration between physicians and industry in the light of potential conflicts of interest, and how patient groups and other stakeholders are involved[191]. Following the submission of new drug applications to regulatory authorities, new drug candidates typically undergo a number of clinical phases (phases 0–IV) to obtain regulatory approval and final marketing authorization. By contrast, the process for medical devices is primarily based on their individual risk profile and invasiveness and does not go through comparable phases. In this context, technologies that are considered low risk may be approved with limited or even without further clinical data, which explains why an early interface between research and development and clinical users is essential to minimize risks and make subsequent regulatory processes as effective and streamlined as possible.

Such considerations of co-development — with a special regard to PAI — were formulated with the appearance of the first breast imaging systems in 2009. Van der Burg highlighted that although PAI was initially developed by the innovative power of engineers to answer their most urgent scientific questions (and to be most successful in their grant applications), a broader range of stakeholders may drive its development in the future[192]. The transfer of intellectual property to companies aiming to capitalize on PAI instruments may further increase the availability of PAI to a greater number of patients, which would lead to PAI being used in clinical applications far beyond those originally envisaged. All stakeholders will then have to decide which (clinical) path to prioritize against the background of limited resources. It remains to be seen whether a specific technological concept or application will bring individual clinical benefits to patients, enable a sustainable business model or, more philosophically, bring benefits to society as a whole.

Apart from this holistic perspective, many concrete ethical problems exist. Several authors have already addressed the question of the

influence of skin colour or melanin content on the accuracy of a PAI measurement[193–196]. This point raises key questions: will the technology be equally accessible to all patients in the future? Which criteria influence the quality of a measurement and therefore the precision of a diagnosis? Should clinical studies include these questions as central issues? A second problem relates to a recurring aspect in medical device development: particularly vulnerable patient groups or those with complex disease, including children, adolescents or pregnant women, are often left out during medical device development for financial reasons. Currently, this is also true for PAI, and research and development are therefore underrepresented in these areas. Another point relates to the possible information content of PAI. Comparing PAI with a conventional ultrasound image, as described above, can offer the physician completely different layers of information. For example, PAI can detect hormonal cycle-related differences in breast tissue[197]. Whether such information is clinically useful is unclear, but it might have an influence (positive or negative) on patients. What if such measurements could predict the likelihood of getting pregnant? Or the risk of breast cancer? Owing to the level of development and maturity of the PAI systems, how valid such information might become is difficult to predict, but a clear framework for future developments is required, including the individual preferences of society, patient groups and other stakeholders. How do they view the advantages and disadvantages? What are their preferences compared with existing procedures? A need exists to involve interest groups and support the development jointly, which is why it seems almost logical that ethical aspects should be considered for future PAI development.

Clinical translation beyond the research setting

Standardization

The wide range of example applications of PAI shows its potential to aid clinical decision-making[38,198–200]. A community-led initiative resulted in the foundation of the International Photoacoustic Standardization Consortium[201] (IPASC) in 2019. The mission of IPASC is to reach consensus on major topics in PAI standardization, to improve the quality of preclinical studies and to accelerate efforts toward clinical translation. By establishing standards, IPASC aims to facilitate the open access, use and exchange of data between different groups to enhance the reproducibility of research. IPASC unites researchers, device developers and government regulators from over 20 countries with more than 130 academic and 30 industrial members.

In 2023, IPASC published findings from a roadmapping exercise that outlines current barriers to the clinical translation of PAI and discusses paths towards its future adoption[202]. One key challenge is that PAI is not a uniform technology, and different manufacturers and research groups have developed diverse hardware and software setups as well as different analytical approaches. PAI systems therefore present a broad range of maturities ('technology readiness levels'), which vary from conceptual ideas or initial proof-of-concept studies to officially cleared (CE certified or FDA approved) devices. This variety explains why the outputs and biomarkers of PAI are neither uniform nor standardized, making results difficult to compare. However, to fully translate PAI to the clinic, image readouts must be consistent and broadly comparable. This problem has been recognized by the scientific community, and the need for sustainable pathways to clinical translation has been intensively discussed[203–205].

In their roadmapping workshop[202], the IPASC identified four thematic areas for future IPASC activity to address major barriers to the clinical translation of PAI: data management, standards development, test objects and methods, and clinical adoption (Box 2 and Table 2).

The PAI community is in a relatively early stage of standardization. From 2018 onwards, IPASC members have gathered information on the technical specifications of PAI systems and produced a consensus document for photoacoustic data and device parameters[206,207]. Identifying a lack of uniformity in PAI data formats, the 'data management theme' then established a data format with a defined consensus metadata structure together with an open-source software application programming interface to enable conversion from proprietary file formats to the IPASC format[207]. If broadly adopted by the community, the IPASC data format could overcome the lack of inter-user data exchange and comparison, which are urgently needed to create comparability across different sites and to enable multicentre clinical trials. These efforts also contributed to the integration of PAI into the Digital Imaging and Communications in Medicine (DICOM) data format, which will be discussed. The next step is building a library of open-source image reconstruction algorithms, compatible with the IPASC data format, that will enable the performance of different reconstruction algorithms to be evaluated under numerous conditions to identify their respective strengths and weaknesses. Such a library is expected to be of growing importance with the increasing use of artificial intelligence in PAI data

Box 2 | Themes of the International Photoacoustic Standardization Consortium

Data management

The data management theme has defined a standard data format and is working towards a sustainable data base for high-quality annotated open-access photoacoustic measurements for education, training and methodological validation.

Standards development

The standards development theme aims to define potential device applications and to design requirements for standardization, along with critical image quality characteristics and quantitative imaging biomarkers. It should establish an interface with, and later gain adoption by, existing standards organizations.

Test objects and methods

For reproducible research and instrument quality assurance and control, the International Photoacoustic Standardization Consortium test objects and methods theme has established consensus on ideal optical and acoustic phantom material properties and is working towards refining geometries. Based on these consensus guidelines, agreed phantom materials and test methods will be refined and disseminated.

Clinical adoption

To promote adoption of photoacoustic imaging (PAI) in the clinic, the PAI community needs to become more outward-facing and more comprehensively consider the needs of healthcare professionals. The clinical adoption theme aims to promote activities to engage the broader clinical community in co-creation to maximize future patient benefit from PAI.

Table 2 | IPASC short-term and long-term missions[202]

Goal	Short-term efforts (<2 years)	Medium-term efforts (2–5 years)	Long-term efforts (>5 years)
Data management roadmap			
Establish a standard data format, develop an open-source software and data framework	Dissemination and consolidation of the IPASC data format Development of a concept for a photoacoustic data base Hardware repeatability tests to understand the limitations of PAI	Create a phantom test platform with varying degrees of complexity Multicentre trials with standardized imaging protocols Implementation of open-access annotated photoacoustic data base	Enrich the data base with a range of PAI data sources and multi-modal images Establish an open-source platform with established data-processing algorithms
Standards development roadmap			
Define potential device applications and requirements for standardization	Define scope of standardization needs and specific objectives Establish a working group/committee within standards organizations to promote standards development Build consensus on phantom requirements, critical image quality and performance characteristics, test methods, and acceptance criteria	Publish and disseminate consensus recommendations and test methods Partner with standard working group to develop official standards through formal consensus building and voting processes under selected standard-developing organizations	Publish the first formal consensus standard for PAI devices Reassess community needs and standardization challenges for future standard editions
Test objects and methods roadmap			
Aid reproducibility of research and instrument quality	Consensus on suitable phantom properties and test methods	Setup of system-specific SOPs Establish and distribute basic precision phantoms Establish phantom protocol (with single-centre and multicentre reproducibility studies)	Universal application of system-specific SOPs Establish and distribute complex accuracy phantoms Commercial manufacturing
Clinical adoption roadmap			
Promote clinical adoption	Define scope of PAI interpretation challenges Identify routes to build consensus on data display Establish working group to create links to clinical education programmes Identify outreach needs in clinical and patient communities	Consensus on image data display schemes for common PAI biomarkers Gather PAI device information and survey community on potential for a 'core engine' Create a diverse portfolio of educational resources for the clinical and patient communities Engagement with broader outreach opportunities to raise the profile of PAI	Coordinate research consortium to obtain funding for design and development of a core engine Integration of PAI concepts into relevant medical training

IPASC, International Photoacoustic Standardization Consortium; PAI, photoacoustic imaging; SOP, standard operating procedure.

processing[208–210]. Software considerations need to be harmonized with possible device applications and design requirements to enable far-reaching standardization.

The 'standards development theme' has worked towards a consensus on 'terms and definitions' in PAI[211], which will guide further IPASC communications and publications. To avoid driving this process in isolation, this theme seeks to create an optimal connection and exchange with formal standards bodies. The effort will also encompass the development and optimization of image quality characteristics and definitions for quantification of imaging biomarkers.

In seeking to maximize the reproducibility of PAI results, the lack of suitable materials and phantoms to enable system validation processes has been recognized; the 'test objects and methods theme' addresses this challenge. Common test objects are widely adopted in other imaging modalities, such as USI, to mimic tissue geometry and properties in order to provide images that correspond to those in living subjects[212]. Similarly, in PAI, test objects should serve three important functions: providing a 'ground truth' of realistic and reproducible data sets, enabling the objective evaluation of the accuracy of particular measurements or signals, and serving in quality assurance and quality control programmes[213]. The current limited availability of test objects, compounded by limited standardization, leads to problems in assessing PAI sensitivity and specificity and creates unwanted uncertainty and potential errors[214]. Standardized test objects or phantoms are thus a keystone for the further development of PAI technologies, enabling precise performance evaluation of imaging systems for research and development as well as clinical translation. Such test procedures should detect degradation in image quality before it impacts diagnostic capacity[212]. Test objects must be made of durable and stable materials, enabling comparable evaluations at different locations and in different systems at the same time[215–218]. Recommendations for a PAI phantom material have now passed IPASC consensus voting and have been published for public consultation[219]; multicentre testing of a stable material that meets these recommendations has been performed at more than 20 sites through the test object and methods theme. The theme has worked to develop traceable and standardized manufacturing processes to produce representative materials with defined properties to mimic real-world conditions[216,220].

Despite these efforts, translation still seems a long way off. However, even without this standardization process, many clinical studies have been published. Perhaps the technical parallels to ultrasound (and the accompanying low risk for the patient) have lowered the barriers to the use of PAI by healthcare professionals and resulted in multicentre studies[221] and studies in children and adolescents[44,142] being conducted at this early stage of PAI development. The IPASC clinical adoption theme is working towards implementing structured

training programmes for medical professionals like those already implemented for other imaging technologies. Without the necessary technical background knowledge (for example, specific PAI artefacts), systematic application errors in clinical routines cannot be excluded. These efforts should involve the broader clinical community for maximum patient benefit.

Regulatory process

The FDA provides multiple approval paths for products, but as PAI does not have a predicate device, a De Novo or Premarket Approval (PMA) path is necessary. The Imagio Breast Imaging system (Seno Medical Instruments Inc.) as a PAUSI system was approved via the PMA path. Prior to the PMA application, feasibility[222] and pilot[223] studies were performed with the Imagio system. For the pivotal clinical trial (PIONEER), 2,105 women with breast masses, identified by screening or palpability, were enrolled after meeting the inclusion criteria[75]. Subsequently, a retrospective clinical study (READER-02)[224] involving 480 patients demonstrated the effectiveness of the Imagio system in differentiating between malignant and benign breast lesions; specificity at a fixed sensitivity of 98% was higher with the Imagio system than with ultrasound alone (47.2% versus 38.2%). The PMA application for the Imagio system was submitted to the FDA.

The PMA application included clinical study data and bench testing data based on custom phantoms, modelling and testing based on existing IEEE standards for ultrasound systems. The phantom study findings included spatial resolution, elevational resolution, uniformity, sensitivity, linearity, dynamic range (SNR and contrast-to-noise ratio), depth detection, out-of-plane optical absorption effects, sO_2 variation, co-registration, precision and geometric distortion[225]. The FDA granted the PMA in January 2021, with supplemental approval in June 2022. Additional USI mode test data were also submitted, as is usual for 510(k) submissions for USI systems. This data includes ultrasound safety and performance data for the USI part of the system, including acoustic output power data, measurement accuracy and diagnostic indications[226].

Demonstrating a significant improvement to an already well-developed diagnostic workflow is challenging. Diagnostic breast imaging generates high volumes, and radiologists have several available imaging modalities. As a new modality, PAI adds information to existing modalities (mammogram, ultrasound and MRI) that can appear confirmatory or contradictory. In the clinical workflow, radiologists tend to look for suspicious findings and then confirm them with biopsy. To improve specificity without an increase in false negatives (loss in sensitivity), radiologists must be able to downgrade suspicion confidently with the additional information provided by PAI. A decision support tool (DST) for the Imagio system was developed to assist radiologists in image interpretation[224]. The DST starts with the user score ultrasound features (for example, peripheral zone, boundary zone, tissue shape, internal texture and sound transmission), photoacoustic features (for example, peripheral radiating vessels, boundary zone vessel, internal vessels, internal Hb and internal blush), and the BI-RADS data and inputs other clinical data (age, lesion size and depth)[221]. The DST then gives a likelihood of malignancy based on the output of artificial intelligence models. For regulatory purposes, the DST is considered part of the device.

In the European Union, regulatory approvals for medical devices have been granted under the Medical Device Directive but the Medical Device Regulation was introduced in 2021, which introduces additional regulatory requirements to manufacturers wishing to market in the European Union and its adoption has generated some challenges. Manufacturers can choose to submit data for approval under the Medical Device Directive during the transitional period, which has been extended to 2027 for high-risk devices and 2028 for lower-risk devices[227].

Some PAI platforms have reached commercialization stage[59,63,65,155,228,229]. The multispectral optoacoustic tomography (MSOT) Acuity Echo (iThera Medical GmbH, Germany), which performs linear-array USTR-based handheld clinical multiwavelength PAI, received the CE mark for European Conformity as a medical device in 2021. Pending regulatory approval for specific clinical applications, MSOT is currently used exclusively in clinical research[163,230,231]. However, in a pivotal step towards commercialization, the multicentre international EUPHORIA study is utilizing MSOT for the diagnosis of inflammatory bowel disease across multiple universities and clinics. Moreover, LME-01 (Luxonus Inc., Japan), a hemispherical-array USTR-based PAI platform, was approved for medical device use in 2022 by Japan's Pharmaceuticals and Medical Devices Agency. In preparation for international regulatory approval, Luxonus is conducting various clinical trials of LME-01 (refs. 59,232,233), including studies in lymphatic and reproductive systems.

The IPASC industry board has added PAI to the DICOM standard as a new imaging modality and, based on the need to appropriately present photoacoustic images to radiologists, a new information object definition has been introduced. DICOM is an international standard for medical images and related information, a format designed to facilitate the exchange of clinically necessary images and related data. As DICOM is implemented in most conventional imaging devices (for example, MRI, CT, PET and ultrasound), numerous DICOM images are in use for clinical diagnosis and treatment. Metadata in DICOM can capture essential parameters related to PAI processes such as patient data, laser settings, imaging geometries, equipment and processing steps. PAI-specific metadata is based on the metadata present in the IPASC data format, allowing translation between the two. The introduction of the DICOM standard can seamlessly address the fundamental problems of PAI standardization, such as data interpretation, storage and sharing, in a vendor-agnostic way. DICOM also forms a framework for communication between PAI and other imaging modalities, storage systems and viewing workstations, expediting the advancement of clinical translation and interoperability of PAI.

The PAUSI procedure has been approved by the American Medical Association and assigned a current procedural terminology (CPT) category III code (0857T) for emerging technologies, effective in 2024. The CPT code is used to describe and report healthcare, surgical and diagnostic services/procedures performed by providers. Healthcare providers use the CPT code for purposes such as billing, reimbursement, regulatory approval, data collection, research and education. The PAUS CPT code includes real-time image documentation and augmentation analysis and/or reporting in the breast and axillary regions. With the assignment of CPT codes, PAI is one step closer to widespread clinical use, enabling clinicians, administrative staff and researchers to collect data to track and improve service quality and quantity.

Outlook

PAI shows remarkable capabilities in visualizing optical contrast with high resolution in tissues, surpassing the limitations of traditional optical imaging technology. PAI can visualize both morphological and functional features in biological tissue, penetrating deeply at the high spatial resolution of USI without the need for exogenous contrast

agents. Moreover, contrast agent-aided photoacoustic molecular imaging can enhance precision medicine, offering a more accurate diagnosis for more effective treatment. Over the past decade, numerous pilot and clinical studies have shown the benefits of PAI for screening, diagnosing and monitoring of diseases in various human organ systems, prompting many engineers and medical professionals to accelerate their efforts toward clinical translation. Research efforts are ongoing to overcome current technical and non-technical limitations and establish standardization and regulatory approval.

Hardware limitations of the laser and the USTR, the main components of the PAI system, affect imaging depth and image quality, but laser sources, system configurations and USTRs are being developed to overcome technical problems. In conjunction with hardware optimization and advancements, research and development are under way in software fields such as image processing. Diverse algorithms are being developed to address precise spectral unmixing, one of the most notable impediments to the clinical translation of PAI[166]. Additionally, efforts are being directed towards the refinement of beamforming algorithms to mitigate limited-view effects and improve spatial resolutions while reconstructing images from photoacoustic signals acquired through USTRs[234]. Moreover, ongoing research is dedicated to the exploration of image processing techniques that effectively suppress or eliminate various artefacts induced by motion, scanning errors and related factors[154,235,236]. Systems using laser diode or LED illumination can benefit from some of these algorithm developments to achieve better image quality at lower cost.

As artificial intelligence finds increasing application in biomedical imaging, artificial intelligence-enhanced PAI is also making major strides[37]. Artificial intelligence technology promises to overcome constraints imposed by both software components (for example, beamforming algorithms and high-throughput data processing[237]) and hardware components (for example, laser specifications and USTR specifications[57,238]). Artificial intelligence technology can also automate image segmentation[239] and classification[106,240] and generate virtually stained pathology images[241,242], thus more efficiently identifying abnormal lesions and improving diagnosis. Integrating artificial intelligence not only overcomes existing limitations but also facilitates the smooth and beneficial application of PAI in clinical settings. Artificial intelligence decision support tools can assist clinicians in interpreting PAI images and reduce interpretation time[224].

For successful clinical translation, PAI must not only achieve hardware and software improvements but also demonstrate a broad and uniform range of maturity. The IPASC has undertaken photoacoustic standardization efforts in four key domains: data management, standards development, test objects and methods, and clinical adoption. This endeavour not only streamlines the regulatory approval process for researchers and manufacturers but also promotes the widespread adoption of PAI devices in medical imaging. To ensure the successful realization of PAI standardization, researchers worldwide must commit to substantial interest and active participation in the standardization efforts. Collaborative engagement from the global research community will contribute to achieving a consensus on PAI standardization and bolster its transformative impact on medical imaging practices.

A major milestone for PAI was reached in 2021, when it obtained FDA approval, demonstrating its potential to enhance diagnostic performance in breast cancer. In 2023, PAI was incorporated into the DICOM standard, marking the beginning of its transformation into a commercially viable medical imaging modality for routine clinical use. The assignment of a CPT code for PAUSI expands health insurance coverage and promotes the social adoption of this new modality.

Published online: 26 September 2024

References

1. Park, Y., Depeursinge, C. & Popescu, G. Quantitative phase imaging in biomedicine. *Nat. Photonics* **12**, 578–589 (2018).
2. Ntziachristos, V. Going deeper than microscopy: the optical imaging frontier in biology. *Nat. Methods* **7**, 603–614 (2010).
3. Yang, S.-T. et al. Carbon dots for optical imaging in vivo. *J. Am. Chem. Soc.* **131**, 11308–11309 (2009).
4. Scholkmann, F. et al. A review on continuous wave functional near-infrared spectroscopy and imaging instrumentation and methodology. *Neuroimage* **85**, 6–27 (2014).
5. Geslien, G. E., Fisher, J. R. & DeLaney, C. Transillumination in breast cancer detection: screening failures and potential. *AJR Am. J. Roentgenol.* **144**, 619–622 (1985).
6. Pichler, B. J., Wehrl, H. F., Kolb, A. & Judenhofer, M. S. Positron emission tomography/magnetic resonance imaging: the next generation of multimodality imaging? *Semin. Nucl. Med.* **38**, 199–208 (2008).
7. Leide-Svegborn, S. Radiation exposure of patients and personnel from a PET/CT procedure with 18F-FDG. *Radiat. Prot. Dosimetry* **139**, 208–213 (2010).
8. Welch, J. N., Johnson, J. A., Bax, M. R., Badr, R. & Shahidi, R. In *IEEE Ultrasonics Symposium Proceedings. An International Symposium (Cat. No. 00CH37121)* 1601–1604 (IEEE, 2000).
9. Beller, S. et al. Image-guided surgery of liver metastases by three-dimensional ultrasound-based optoelectronic navigation. *J. Br. Surg.* **94**, 866–875 (2007).
10. Gill, R. W. Measurement of blood flow by ultrasound: accuracy and sources of error. *Ultrasound Med. Biol.* **11**, 625–641 (1985).
11. Sigrist, R. M., Liau, J., El Kaffas, A., Chammas, M. C. & Willmann, J. K. Ultrasound elastography: review of techniques and clinical applications. *Theranostics* **7**, 1303 (2017).
12. Zhang, P. et al. High-resolution deep functional imaging of the whole mouse brain by photoacoustic computed tomography in vivo. *J. Biophotonics* **11**, e201700024 (2018).
13. Wang, L. V. & Hu, S. Photoacoustic tomography: in vivo imaging from organelles to organs. *Science* **335**, 1458–1462 (2012).
14. Choi, W. et al. Recent advances in contrast-enhanced photoacoustic imaging: overcoming the physical and practical challenges. *Chem. Rev.* **123**, 7379–7419 (2023).
15. Kim, J. et al. Programmable real-time clinical photoacoustic and ultrasound imaging system. *Sci. Rep.* **6**, 35137 (2016).
16. Wen, Y. et al. Clinical photoacoustic/ultrasound dual-modal imaging: current status and future trends. *Front. Physiol.* **13**, 2227 (2022).
17. Bell, A. G. The photophone. *Science* **1**, 130–134 (1880).
18. Vengerov, M. An optical-acoustic method of gas analysis. *Nature* **158**, 28–29 (1946).
19. Delany, M. E. The optic-acoustic effect in gases. *Sci. Prog.* **47**, 459–467 (1959).
20. Rosencwaig, A. Photoacoustic spectroscopy of solids. *Opt. Commun.* **7**, 305–308 (1973).
21. Busse, G. & Rosencwaig, A. Subsurface imaging with photoacoustics. *Appl. Phys. Lett.* **36**, 815–816 (1980).
22. Wada, K. et al. Laser photoacoustic microscopy for the determination of dye on a solid biopolymer. *Chem. Pharm. Bull.* **33**, 1316–1319 (1985).
23. Wada, K., Masujima, T., Yoshida, H. & Imai, H. Photoacoustic microscopy for the analysis of peroxidase activity in a biological tissue. *Chem. Pharm. Bull.* **34**, 1834–1836 (1986).
24. Diebold, G., Sun, T. & Khan, M. Photoacoustic monopole radiation in one, two, and three dimensions. *Phys. Rev. Lett.* **67**, 3384 (1991).
25. Oraevsky, A. A., Jacques, S. L., Esenaliev, R. O. & Tittel, F. K. In *Laser-Tissue Interaction V; and Ultraviolet Radiation Hazards* 122–128 (SPIE, 1994).
26. Kruger, R. A. Photoacoustic ultrasound. *Med. Phys.* **21**, 127–131 (1994).
27. Manohar, S. & Razansky, D. Photoacoustics: a historical review. *Adv. Opt. Photonics* **8**, 586–617 (2016).
28. Savateeva, E. V. et al. In *Biomedical Optoacoustics* 55–66 (SPIE, 2000).
29. Wang, X. et al. Noninvasive laser-induced photoacoustic tomography for structural and functional in vivo imaging of the brain. *Nat. Biotechnol.* **21**, 803–806 (2003).
30. Oraevsky, A. A. et al. In *Biomedical Optoacoustics II* 6–15 (SPIE, 2001).
31. Taruttis, A. & Ntziachristos, V. Advances in real-time multispectral optoacoustic imaging and its applications. *Nat. Photonics* **9**, 219–227 (2015).
32. Park, B., Oh, D., Kim, J. & Kim, C. Functional photoacoustic imaging: from nano- and micro- to macro-scale. *Nano Converg.* **10**, 29 (2023).
33. Park, B., Kim, C. & Kim, J. Recent advances in ultrasound and photoacoustic analysis for thyroid cancer diagnosis. *Adv. Phys. Res.* **2**, 2200070 (2023).
34. Park, E.-Y., Lee, H., Han, S., Kim, C. & Kim, J. Photoacoustic imaging systems based on clinical ultrasound platform. *Exp. Biol. Med.* **247**, 551–560 (2022).
35. Lee, C., Kim, C. & Park, B. Review of three-dimensional handheld photoacoustic and ultrasound imaging systems and their applications. *Sensors* **23**, 8149 (2023).
36. Yang, J., Choi, S. & Kim, C. Practical review on photoacoustic computed tomography using curved ultrasound array transducer. *Biomed. Eng. Lett.* **12**, 19–35 (2021).
37. Yang, J., Choi, S., Kim, J., Park, B. & Kim, C. Recent advances in deep-learning-enhanced photoacoustic imaging. *Adv. Photonics Nexus* **2**, 054001 (2023).
38. Attia, A. B. E. et al. A review of clinical photoacoustic imaging: current and future trends. *Photoacoustics* **16**, 100144 (2019).
39. Zhang, H. F., Maslov, K., Stoica, G. & Wang, L. V. Functional photoacoustic microscopy for high-resolution and noninvasive in vivo imaging. *Nat. Biotechnol.* **24**, 848–851 (2006).

40. Park, B. et al. 3D wide-field multispectral photoacoustic imaging of human melanomas in vivo: a pilot study. *J. Eur. Acad. Dermatol. Venereol.* **35**, 669–676 (2021).
41. Shi, J. et al. High-resolution, high-contrast mid-infrared imaging of fresh biological samples with ultraviolet-localized photoacoustic microscopy. *Nat. Photonics* **13**, 609–615 (2019).
42. Baik, J. W. et al. Intraoperative label-free photoacoustic histopathology of clinical specimens. *Laser Photonics Rev.* **15**, 2100124 (2021).
43. Fasoula, N.-A. et al. Non-invasive multispectral optoacoustic tomography resolves intrahepatic lipids in patients with hepatic steatosis. *Photoacoustics* **29**, 100454 (2023).
44. Regensburger, A. P. et al. Detection of collagens by multispectral optoacoustic tomography as an imaging biomarker for Duchenne muscular dystrophy. *Nat. Med.* **25**, 1905–1915 (2019).
45. Weber, J., Beard, P. C. & Bohndiek, S. E. Contrast agents for molecular photoacoustic imaging. *Nat. Methods* **13**, 639–650 (2016).
46. Yao, J. et al. High-speed label-free functional photoacoustic microscopy of mouse brain in action. *Nat. Methods* **12**, 407–410 (2015).
47. Kim, J. et al. Multiparametric photoacoustic analysis of human thyroid cancers in vivophotoacoustic analysis of human thyroid cancers. *Cancer Res.* **81**, 4849–4860 (2021).
48. Yao, J., Maslov, K. I., Shi, Y., Taber, L. A. & Wang, L. V. In vivo photoacoustic imaging of transverse blood flow by using Doppler broadening of bandwidth. *Opt. Lett.* **35**, 1419–1421 (2010).
49. Singh, M. S. & Thomas, A. Photoacoustic elastography imaging: a review. *J. Biomed. Opt.* **24**, 040902 (2019).
50. Yao, J. et al. Noninvasive photoacoustic computed tomography of mouse brain metabolism in vivo. *Neuroimage* **64**, 257–266 (2013).
51. Kim, C., Song, K. H., Gao, F. & Wang, L. V. Sentinel lymph nodes and lymphatic vessels: noninvasive dual-modality in vivo mapping by using indocyanine green in rats — volumetric spectroscopic photoacoustic imaging and planar fluorescence imaging. *Radiology* **255**, 442–450 (2010).
52. Cox, B. T. & Treeby, B. E. Artifact trapping during time reversal photoacoustic imaging for acoustically heterogeneous media. *IEEE Trans. Med. Imaging* **29**, 387–396 (2009).
53. Jeon, S. et al. Real-time delay-multiply-and-sum beamforming with coherence factor for in vivo clinical photoacoustic imaging of humans. *Photoacoustics* **15**, 100136 (2019).
54. Jeng, G.-S. et al. Real-time interleaved spectroscopic photoacoustic and ultrasound (PAUS) scanning with simultaneous fluence compensation and motion correction. *Nat. Commun.* **12**, 716 (2021).
55. Puglisi, J. D. & Tinoco Jr, I. In *Methods in Enzymology* 180, 304–325 (Elsevier, 1989).
56. Stoscheck, C. M. In *Methods in Enzymology* 182, 50–68 (Elsevier, 1990).
57. Choi, S. et al. Deep learning enhances multiparametric dynamic volumetric photoacoustic computed tomography in vivo (DL-PACT). *Adv. Sci.* **10**, 2202089 (2023).
58. Lv, J., Xu, Y., Xu, L. & Nie, L. Quantitative functional evaluation of liver fibrosis in mice with dynamic contrast-enhanced photoacoustic imaging. *Radiology* **300**, 89–97 (2021).
59. Suzuki, Y. et al. Subcutaneous lymphatic vessels in the lower extremities: comparison between photoacoustic lymphangiography and near-infrared fluorescence lymphangiography. *Radiology* **295**, 469–474 (2020).
60. Paulus, L. P. et al. Contrast-enhanced multispectral optoacoustic tomography for functional assessment of the gastrointestinal tract. *Adv. Sci.* **10**, e2302562 (2023).
61. Feng, T. et al. Detection of collagen by multi-wavelength photoacoustic analysis as a biomarker for bone health assessment. *Photoacoustics* **24**, 100296 (2021).
62. Nagae, K. et al. Real-time 3D photoacoustic visualization system with a wide field of view for imaging human limbs. *F1000Res* **7**, 1813 (2018).
63. Lei, S. et al. In vivo three-dimensional multispectral photoacoustic imaging of dual enzyme-driven cyclic cascade reaction for tumor catalytic therapy. *Nat. Commun.* **13**, 1298 (2022).
64. Paltauf, G., Nuster, R. & Frenz, M. Progress in biomedical photoacoustic imaging instrumentation toward clinical application. *J. Appl. Phys.* **128**, 180907 (2020).
65. Oraevsky, A. et al. In *Photons Plus Ultrasound: Imaging and Sensing* 217–226 (SPIE, 2018).
66. Neuschler, E. I. et al. A pivotal study of optoacoustic imaging to diagnose benign and malignant breast masses: a new evaluation tool for radiologists. *Radiology* **287**, 398–412 (2017).
67. Taruttis, A. et al. Optoacoustic imaging of human vasculature: feasibility by using a handheld probe. *Radiology* **281**, 256–263 (2016).
68. Knieling, F. et al. Raster-scanning optoacoustic mesoscopy for gastrointestinal imaging at high resolution. *Gastroenterology* **154**, 807–809.e3 (2018).
69. Ahn, J., Kim, J. Y., Choi, W. & Kim, C. High-resolution functional photoacoustic monitoring of vascular dynamics in human fingers. *Photoacoustics* **23**, 100282 (2021).
70. Wang, L. V. & Yao, J. A practical guide to photoacoustic tomography in the life sciences. *Nat. Methods* **13**, 627–638 (2016).
71. Choi, W., Park, E.-Y., Jeon, S. & Kim, C. Clinical photoacoustic imaging platforms. *Biomed. Eng. Lett.* **8**, 139–155 (2018).
72. Basij, M. et al. Miniaturized phased-array ultrasound and photoacoustic endoscopic imaging system. *Photoacoustics* **15**, 100139 (2019).
73. Neuschmelting, V. et al. Performance of a multispectral optoacoustic tomography (MSOT) system equipped with 2D vs. 3D handheld probes for potential clinical translation. *Photoacoustics* **4**, 1–10 (2016).
74. Kim, J. et al. Multiparametric photoacoustic analysis of human thyroid cancers in vivo. *Cancer Res.* **81**, 4849–4860 (2021).
75. Neuschler, E. I. et al. A pivotal study of optoacoustic imaging to diagnose benign and malignant breast masses: a new evaluation tool for radiologists. *Radiology* **287**, 398–412 (2018).
76. Choi, W. et al. Three-dimensional multistructural quantitative photoacoustic and US imaging of human feet in vivo. *Radiology* **303**, 467–473 (2022).
77. Oraevsky, A. et al. Clinical optoacoustic imaging combined with ultrasound for coregistered functional and anatomical mapping of breast tumors. *Photoacoustics* **12**, 30–45 (2018).
78. Liu, C. et al. In vivo transrectal imaging of canine prostate with a sensitive and compact handheld transrectal array photoacoustic probe for early diagnosis of prostate cancer. *Biomed. Opt. Express* **10**, 1707–1717 (2019).
79. Kothapalli, S.-R. et al. Simultaneous transrectal ultrasound and photoacoustic human prostate imaging. *Sci. Transl. Med.* **11**, eaav2169 (2019).
80. Asao, Y. et al. Photoacoustic mammography capable of simultaneously acquiring photoacoustic and ultrasound images. *J. Biomed. Opt.* **21**, 116009 (2016).
81. Lin, L. et al. Single-breath-hold photoacoustic computed tomography of the breast. *Nat. Commun.* **9**, 2352 (2018).
82. Chitgupi, U. et al. Surfactant-stripped micelles for NIR-II photoacoustic imaging through 12 cm of breast tissue and whole human breasts. *Adv. Mater.* **31**, 1902279 (2019).
83. Na, S. et al. Massively parallel functional photoacoustic computed tomography of the human brain. *Nat. Biomed. Eng.* **6**, 584–592 (2022).
84. Toi, M. et al. Visualization of tumor-related blood vessels in human breast by photoacoustic imaging system with a hemispherical detector array. *Sci. Rep.* **7**, 41970 (2017).
85. He, H. et al. Fast raster-scan optoacoustic mesoscopy enables assessment of human melanoma microvasculature in vivo. *Nat. Commun.* **13**, 2803 (2022).
86. Aguirre, J. et al. Precision assessment of label-free psoriasis biomarkers with ultra-broadband optoacoustic mesoscopy. *Nat. Biomed. Eng.* **1**, 0068 (2017).
87. Hindelang, B. et al. Enabling precision monitoring of psoriasis treatment by optoacoustic mesoscopy. *Sci. Transl. Med.* **14**, eabm8059 (2022).
88. Mogensen, M., Thrane, L., Jørgensen, T. M., Andersen, P. E. & Jemec, G. B. OCT imaging of skin cancer and other dermatological diseases. *J. Biophotonics* **2**, 442–451 (2009).
89. Koller, S. et al. In vivo reflectance confocal microscopy of erythematosquamous skin diseases. *Exp. Dermatol.* **18**, 536–540 (2009).
90. König, K. et al. Translation of two-photon microscopy to the clinic: multimodal multiphoton CARS tomography of in vivo human skin. *J. Biomed. Opt.* **25**, 014515 (2020).
91. Bhatta, A. K., Keyal, U. & Liu, Y. Application of high frequency ultrasound in dermatology. *Discov. Med.* **26**, 237–242 (2018).
92. Attia, A. B. E. et al. Noninvasive real-time characterization of non-melanoma skin cancers with handheld optoacoustic probes. *Photoacoustics* **7**, 20–26 (2017).
93. Chuah, S. et al. Structural and functional 3D mapping of skin tumours with non-invasive multispectral optoacoustic tomography. *Skin Res. Technol.* **23**, 221–226 (2017).
94. Ford, S. J. et al. Structural and functional analysis of intact hair follicles and pilosebaceous units by volumetric multispectral optoacoustic tomography. *J. Invest. Dermatol.* **136**, 753–761 (2016).
95. Zhou, Y. et al. Handheld photoacoustic probe to detect both melanoma depth and volume at high speed in vivo. *J. Biophotonics* **8**, 961–967 (2015).
96. Zhou, Y. et al. Noninvasive determination of melanoma depth using a handheld photoacoustic probe. *J. Invest. Dermatol.* **137**, 1370 (2017).
97. Langley, R. G. & Ellis, C. N. Evaluating psoriasis with psoriasis area and severity index, psoriasis global assessment, and lattice system physician's global assessment. *J. Am. Acad. Dermatol.* **51**, 563–569 (2004).
98. Oji, V. & Luger, T. A. The skin in psoriasis: assessment and challenges. *Clin. Exp. Rheumatol.* **33**, S14–19 (2015).
99. Ashcroft, D., Li Wan Po, A., Williams, H. & Griffiths, C. Clinical measures of disease severity and outcome in psoriasis: a critical appraisal of their quality. *Br. J. Dermatol.* **141**, 185–191 (1999).
100. Marks, R. Measurement of the response to treatment in psoriasis. *J. Dermatol. Treat.* **7**, S7–S10 (1996).
101. Griffiths, C. E. & Barker, J. N. Pathogenesis and clinical features of psoriasis. *Lancet* **370**, 263–271 (2007).
102. Ryan, C. et al. Research gaps in psoriasis: opportunities for future studies. *J. Am. Acad. Dermatol.* **70**, 146–167 (2014).
103. He, H. et al. Machine learning analysis of human skin by optoacoustic mesoscopy for automated extraction of psoriasis and aging biomarkers. *IEEE Trans. Med. Imaging* **43**, 2074–2085 (2024).
104. Masthoff, M. et al. Multispectral optoacoustic tomography of systemic sclerosis. *J. Biophotonics* **11**, e201800155 (2018).
105. Wilkinson, S. et al. Photoacoustic imaging is a novel tool to measure finger artery structure and oxygenation in patients with SSc. *Sci. Rep.* **12**, 20446 (2022).
106. Nitkunanantharajah, S. et al. Three-dimensional optoacoustic imaging of nailfold capillaries in systemic sclerosis and its potential for disease differentiation using deep learning. *Sci. Rep.* **10**, 16444 (2020).
107. Eisenbrey, J. R., Stanczak, M., Forsberg, F., Mendoza-Ballesteros, F. A. & Lyshchik, A. Photoacoustic oxygenation quantification in patients with Raynaud's: first-in-human results. *Ultrasound Med. Biol.* **44**, 2081–2088 (2018).
108. Yew, Y. W. et al. Investigation of morphological, vascular and biochemical changes in the skin of an atopic dermatitis (AD) patient in response to dupilumab using raster scanning optoacoustic mesoscopy (RSOM) and handheld confocal Raman spectroscopy (CRS). *J. Dermatol. Sci.* **95**, 123–125 (2019).

109. Yew, Y. W. et al. Raster-scanning optoacoustic mesoscopy imaging as an objective disease severity tool in atopic dermatitis patients. *J. Am. Acad. Dermatol.* **84**, 1121–1123 (2021).
110. Park, S. et al. Model learning analysis of 3D optoacoustic mesoscopy images for the classification of atopic dermatitis. *Biomed. Opt. Express* **12**, 3671–3683 (2021).
111. Li, X. et al. Multispectral raster-scanning optoacoustic mesoscopy differentiate lesional from non-lesional atopic dermatitis skin using structural and functional imaging markers. *Photoacoustics* **28**, 100399 (2022).
112. Nau, T. et al. Raster-scanning optoacoustic mesoscopy biomarkers for atopic dermatitis skin lesions. *Photoacoustics* **31**, 100513 (2023).
113. Hindelang, B. et al. Optoacoustic mesoscopy shows potential to increase accuracy of allergy patch testing. *Contact Dermat.* **83**, 206–214 (2020).
114. Gonzalez, E. A. & Bell, M. A. L. Photoacoustic imaging and characterization of bone in medicine: overview, applications, and outlook. *Annu. Rev. Biomed. Eng.* **25**, 207–232 (2023).
115. Chamberland, D. L., Wang, X. & Roessler, B. J. Photoacoustic tomography of carrageenan-induced arthritis in a rat model. *J. Biomed. Opt.* **13**, 011006 (2008).
116. Rajian, J. R., Shao, X., Chamberland, D. L. & Wang, X. Characterization and treatment monitoring of inflammatory arthritis by photoacoustic imaging: a study on adjuvant-induced arthritis rat model. *Biomed. Opt. Express* **4**, 900–908 (2013).
117. Lutzweiler, C., Meier, R., Rummeny, E., Ntziachristos, V. & Razansky, D. Real-time optoacoustic tomography of indocyanine green perfusion and oxygenation parameters in human finger vasculature. *Opt. Lett.* **39**, 4061–4064 (2014).
118. Keswani, R. K. et al. Repositioning clofazimine as a macrophage-targeting photoacoustic contrast agent. *Sci. Rep.* **6**, 23528 (2016).
119. Wang, X., Chamberland, D. L. & Jamadar, D. A. Noninvasive photoacoustic tomography of human peripheral joints toward diagnosis of inflammatory arthritis. *Opt. Lett.* **32**, 3002–3004 (2007).
120. Sun, Y., Sobel, E. & Jiang, H. Quantitative three-dimensional photoacoustic tomography of the finger joints: an in vivo study. *J. Biomed. Opt.* **14**, 064005 (2009).
121. Xi, L. & Jiang, H. High resolution three-dimensional photoacoustic imaging of human finger joints in vivo. *Appl. Phys. Lett.* **107**, 063701 (2015).
122. van Es, P., Biswas, S. K., Moens, H. J. B., Steenbergen, W. & Manohar, S. Initial results of finger imaging using photoacoustic computed tomography. *J. Biomed. Opt.* **19**, 060501 (2014).
123. Xu, G. et al. Photoacoustic and ultrasound dual-modality imaging of human peripheral joints. *J. Biomed. Opt.* **18**, 010502 (2013).
124. Yuan, J. et al. Real-time photoacoustic and ultrasound dual-modality imaging system facilitated with graphics processing unit and code parallel optimization. *J. Biomed. Opt.* **18**, 086001 (2013).
125. Xiao, J. et al. Quantitative two-dimensional photoacoustic tomography of osteoarthritis in the finger joints. *Opt. Express* **18**, 14359–14365 (2010).
126. van Es, P. et al. In *European Conference on Biomedical Optics* 95390C (Optica Publishing Group, 2015).
127. Jo, J. et al. A functional study of human inflammatory arthritis using photoacoustic imaging. *Sci. Rep.* **7**, 15026 (2017).
128. Zhao, C. et al. Multimodal photoacoustic/ultrasonic imaging system: a promising imaging method for the evaluation of disease activity in rheumatoid arthritis. *Eur. Radiol.* **31**, 3542–3552 (2021).
129. Yang, M. et al. Synovial oxygenation at photoacoustic imaging to assess rheumatoid arthritis disease activity. *Radiology* **306**, 220–228 (2023).
130. Kapuku, G. K. & Kop, W. J. In *Handbook of Cardiovascular Behavioral Medicine* 45–80 (Springer Nature, 2022).
131. Günther, J. S. et al. Targeting muscular hemoglobin content for classification of peripheral arterial disease by noninvasive multispectral optoacoustic tomography. *Cardiovasc. Imaging* **16**, 719–721 (2023).
132. Masthoff, M. et al. Use of multispectral optoacoustic tomography to diagnose vascular malformations. *JAMA Dermatol.* **154**, 1457–1462 (2018).
133. Muller, J.-W. et al. Towards in vivo photoacoustic imaging of vulnerable plaques in the carotid artery. *Biomed. Opt. Express* **12**, 4207–4218 (2021).
134. Ivankovic, I., Merčep, E., Schmedt, C.-G., Deán-Ben, X. L. & Razansky, D. Real-time volumetric assessment of the human carotid artery: handheld multispectral optoacoustic tomography. *Radiology* **291**, 45–50 (2019).
135. Karlas, A. et al. Multispectral optoacoustic tomography of lipid and hemoglobin contrast in human carotid atherosclerosis. *Photoacoustics* **23**, 100283 (2021).
136. Ganzleben, I. et al. Multispectral optoacoustic tomography for the non-invasive identification of patients with severe anemia in vivo. *Photoacoustics* **28**, 100414 (2022).
137. Grünherz, L. et al. Preoperative mapping of lymphatic vessels by multispectral optoacoustic tomography. *Lymphatic Res. Biol.* **20**, 659–664 (2022).
138. Giacalone, G., Yamamoto, T., Belva, F. & Hayashi, A. Bedside 3D visualization of lymphatic vessels with a handheld multispectral optoacoustic tomography device. *J. Clin. Med.* **9**, 815 (2020).
139. Ahmed, M., Purushotham, A. D. & Douek, M. Novel techniques for sentinel lymph node biopsy in breast cancer: a systematic review. *Lancet Oncol.* **15**, e351–e362 (2014).
140. Stoffels, I. et al. Metastatic status of sentinel lymph nodes in melanoma determined noninvasively with multispectral optoacoustic imaging. *Sci. Transl. Med.* **7**, 317ra199 (2015).
141. Stoffels, I. et al. Assessment of nonradioactive multispectral optoacoustic tomographic imaging with conventional lymphoscintigraphic imaging for sentinel lymph node biopsy in melanoma. *JAMA Netw. Open* **2**, e199020 (2019).
142. Regensburger, A. P. et al. Multispectral optoacoustic tomography for non-invasive disease phenotyping in pediatric spinal muscular atrophy patients. *Photoacoustics* **25**, 100315 (2022).
143. Wagner, A. L. et al. Noninvasive imaging in pediatric spinal muscular atrophy patients using multispectral optoacoustic tomography: a proof-of-concept study. *Neuropediatrics* **52**, S1–S53 (2021).
144. Karlas, A., Pleitez, M. A., Aguirre, J. & Ntziachristos, V. Optoacoustic imaging in endocrinology and metabolism. *Nat. Rev. Endocrinol.* **17**, 323–335 (2021).
145. Roll, W. et al. Multispectral optoacoustic tomography of benign and malignant thyroid disorders: a pilot study. *J. Nucl. Med.* **60**, 1461–1466 (2019).
146. He, H. et al. Opening a window to skin biomarkers for diabetes stage with optoacoustic mesoscopy. *Light Sci. Appl.* **12**, 231 (2023).
147. Karlas, A. et al. Dermal features derived from optoacoustic tomograms via machine learning correlate microangiopathy phenotypes with diabetes stage. *Nat. Biomed. Eng.* **7**, 1667–1682 (2023).
148. Knieling, F. et al. Multispectral optoacoustic tomography for assessment of Crohn's disease activity. *N. Engl. J. Med.* **376**, 1292–1294 (2017).
149. Knieling, F. et al. Multispectral optoacoustic tomography in ulcerative colitis — a first-in-human diagnostic clinical trial. *J. Nucl. Med.* **58**, 1196 (2017).
150. Regensburger, A. P. et al. Multispectral optoacoustic tomography enables assessment of disease activity in paediatric inflammatory bowel disease. *Photoacoustics* **35**, 100578 (2024).
151. Ni, L. et al. Assessment of prostate cancer progression using a translational needle photoacoustic sensing probe: preliminary study with intact human prostates ex-vivo. *Photoacoustics* **28**, 100418 (2022).
152. Abeyakoon, O. et al. An optoacoustic imaging feature set to characterise blood vessels surrounding benign and malignant breast lesions. *Photoacoustics* **27**, 100383 (2022).
153. Manohar, S. & Dantuma, M. Current and future trends in photoacoustic breast imaging. *Photoacoustics* **16**, 100134 (2019).
154. Lin, L. et al. Photoacoustic computed tomography of breast cancer in response to neoadjuvant chemotherapy. *Adv. Sci.* **8**, 2003396 (2021).
155. Schoustra, S. M. et al. Twente photoacoustic mammoscope 2: system overview and three-dimensional vascular network images in healthy breasts. *J. Biomed. Opt.* **24**, 121909 (2019).
156. Jafari, S. H. et al. Breast cancer diagnosis: imaging techniques and biochemical markers. *J. Cell. Physiol.* **233**, 5200–5213 (2018).
157. Piras, D., Xia, W., Steenbergen, W., Van Leeuwen, T. G. & Manohar, S. Photoacoustic imaging of the breast using the Twente photoacoustic mammoscope: present status and future perspectives. *IEEE J. Sel. Top. Quantum Electron.* **16**, 730–739 (2009).
158. Nyayapathi, N. et al. Dual scan mammoscope (DSM) — a new portable photoacoustic breast imaging system with scanning in craniocaudal plane. *IEEE Trans. Biomed. Eng.* **67**, 1321–1327 (2019).
159. Li, X., Heldermon, C. D., Yao, L., Xi, L. & Jiang, H. High resolution functional photoacoustic tomography of breast cancer. *Med. Phys.* **42**, 5321–5328 (2015).
160. Deán-Ben, X. L., Fehm, T. F., Gostic, M. & Razansky, D. Volumetric hand-held optoacoustic angiography as a tool for real-time screening of dense breast. *J. Biophotonics* **9**, 253–259 (2016).
161. Diot, G. et al. Multispectral optoacoustic tomography (MSOT) of human breast cancer. *Clin. Cancer Res.* **23**, 6912–6922 (2017).
162. Vonk, J. et al. Multispectral optoacoustic tomography for in vivo detection of lymph node metastases in oral cancer patients using an EGFR-targeted contrast agent and intrinsic tissue contrast: a proof-of-concept study. *Photoacoustics* **26**, 100362 (2022).
163. Noltes, M. E. et al. Towards in vivo characterization of thyroid nodules suspicious for malignancy using multispectral optoacoustic tomography. *Eur. J. Nucl. Med. Mol. Imaging* **50**, 2736–2750 (2023).
164. Sharma, A., Srishti, Periyasamy, V. & Pramanik, M. Photoacoustic imaging depth comparison at 532-, 800-, and 1064-nm wavelengths: monte Carlo simulation and experimental validation. *J. Biomed. Opt.* **24**, 121904 (2019).
165. Manwar, R., Lara, J. B., Prakash, R., Ranjbaran, S. M. & Avanaki, K. Randomized multi-angle illumination for improved linear array photoacoustic computed tomography in brain. *J. Biophotonics* **15**, e202200016 (2022).
166. Tzoumas, S. et al. Eigenspectra optoacoustic tomography achieves quantitative blood oxygenation imaging deep in tissues. *Nat. Commun.* **7**, 12121 (2016).
167. Kirillin, M., Perekatova, V., Turchin, I. & Subochev, P. Fluence compensation in raster-scan optoacoustic angiography. *Photoacoustics* **8**, 59–67 (2017).
168. Choi, W., Oh, D. & Kim, C. Practical photoacoustic tomography: realistic limitations and technical solutions. *J. Appl. Phys.* **127**, 230903 (2020).
169. Chandramoorthi, S., Riksen, J. J., Nikolaev, A. V., Van Der Steen, A. F. & Van Soest, G. Wideband photoacoustic imaging in vivo with complementary frequency conventional ultrasound transducers. *Front. Phys.* https://doi.org/10.3389/fphy.2022.954537 (2022).
170. Joseph, J., Ma, B. & Khuri-Yakub, B. Applications of capacitive micromachined ultrasonic transducers: a comprehensive review. *IEEE Trans. Ultrason. Ferroelectr. Freq. Control* **69**, 456–467 (2021).
171. Jung, J. et al. Review of piezoelectric micromachined ultrasonic transducers and their applications. *J. Micromech. Microeng.* **27**, 113001 (2017).
172. Manwar, R., Kratkiewicz, K. & Avanaki, K. Overview of ultrasound detection technologies for photoacoustic imaging. *Micromachines* **11**, 692 (2020).
173. Vallet, M. et al. Quantitative comparison of PZT and CMUT probes for photoacoustic imaging: experimental validation. *Photoacoustics* **8**, 48–58 (2017).

174. Park, J. et al. Quadruple ultrasound, photoacoustic, optical coherence, and fluorescence fusion imaging with a transparent ultrasound transducer. *Proc. Natl Acad. Sci. USA* **118**, e1920879118 (2021).
175. Chen, H. et al. A transparent ultrasound array for real-time optical, ultrasound, and photoacoustic imaging. *BME Front.* **2022**, 9871098 (2022).
176. Ilkhechi, A. K., Ceroici, C., Li, Z. & Zemp, R. Transparent capacitive micromachined ultrasonic transducer (CMUT) arrays for real-time photoacoustic applications. *Opt. express* **28**, 13750–13760 (2020).
177. Ansari, R., Zhang, E. Z., Desjardins, A. E. & Beard, P. C. All-optical forward-viewing photoacoustic probe for high-resolution 3D endoscopy. *Light Sci. Appl.* **7**, 75 (2018).
178. Zhang, E., Laufer, J. & Beard, P. Backward-mode multiwavelength photoacoustic scanner using a planar Fabry-Perot polymer film ultrasound sensor for high-resolution three-dimensional imaging of biological tissues. *Appl. Opt.* **47**, 561–577 (2008).
179. Ashkenazi, S., Chao, C.-Y., Guo, L. J. & O'Donnell, M. Ultrasound detection using polymer microring optical resonator. *Appl. Phys. Lett.* **85**, 5418–5420 (2004).
180. Li, H., Dong, B., Zhang, Z., Zhang, H. F. & Sun, C. A transparent broadband ultrasonic detector based on an optical micro-ring resonator for photoacoustic microscopy. *Sci. Rep.* **4**, 4496 (2014).
181. Hazan, Y., Levi, A., Nagli, M. & Rosenthal, A. Silicon-photonics acoustic detector for optoacoustic micro-tomography. *Nat. Commun.* **13**, 1488 (2022).
182. Shnaiderman, R. et al. A submicrometre silicon-on-insulator resonator for ultrasound detection. *Nature* **585**, 372–378 (2020).
183. Boktor, M. et al. Virtual histological staining of label-free total absorption photoacoustic remote sensing (TA-PARS). *Sci. Rep.* **12**, 10296 (2022).
184. Ecclestone, B. R. et al. Label-free complete absorption microscopy using second generation photoacoustic remote sensing. *Sci. Rep.* **12**, 8464 (2022).
185. Daoudi, K. et al. Handheld probe integrating laser diode and ultrasound transducer array for ultrasound/photoacoustic dual modality imaging. *Opt. Express* **22**, 26365–26374 (2014).
186. Hariri, A. et al. The characterization of an economic and portable LED-based photoacoustic imaging system to facilitate molecular imaging. *Photoacoustics* **9**, 10–20 (2018).
187. Zissis, G., Bertoldi, P. & Serrenho, T. *Update on the Status of LED-Lighting World Market Since 2018* (Publications Office of the European Union, 2021).
188. Li, L. The advances and characteristics of high-power diode laser materials processing. *Opt. Lasers Eng.* **34**, 231–253 (2000).
189. Baribeau, Y. et al. Handheld point-of-care ultrasound probes: the new generation of POCUS. *J. Cardiothorac. Vasc. Anesthesia* **34**, 3139–3145 (2020).
190. European Society of Radiology (ESR). Renewal of radiological equipment. *Insights Imaging* **5**, 543–546 (2014).
191. Citron, P. Ethics considerations for medical device R&D. *Prog. Cardiovasc. Dis.* **55**, 307–315 (2012).
192. Van der Burg, S. Imagining the future of photoacoustic mammography. *Sci. Eng. Ethics* **15**, 97–110 (2009).
193. Mantri, Y. & Jokerst, J. V. Impact of skin tone on photoacoustic oximetry and tools to minimize bias. *Biomed. Opt. Express* **13**, 875–887 (2022).
194. Else, T. R. et al. Effects of skin tone on photoacoustic imaging and oximetry. *J. Biomed. Opt.* **29**, S11506 (2024).
195. Fernandes, G. S. et al. Mitigating skin tone bias in linear array in vivo photoacoustic imaging with short-lag spatial coherence beamforming. *Photoacoustics* **33**, 100555 (2023).
196. Vogt, W. C., Wear, K. A. & Pfefer, T. J. Phantoms for evaluating the impact of skin pigmentation on photoacoustic imaging and oximetry performance. *Biomed. Opt. Express* **14**, 5735–5748 (2023).
197. Abeyakoon, O. et al. Optoacoustic imaging detects hormone-related physiological changes of breast parenchyma. *Ultraschall Med.* **40**, 757–763 (2019).
198. Steinberg, I. et al. Photoacoustic clinical imaging. *Photoacoustics* **14**, 77–98 (2019).
199. Upputuri, P. K. & Pramanik, M. Recent advances toward preclinical and clinical translation of photoacoustic tomography: a review. *J. Biomed. Opt.* **22**, 41006 (2017).
200. Schellenberg, M. W. & Hunt, H. K. Hand-held optoacoustic imaging: a review. *Photoacoustics* **11**, 14–27 (2018).
201. Bohndiek, S. Addressing photoacoustics standards. *Nat. Photonics* **13**, 298 (2019).
202. Assi, H. et al. A review of a strategic roadmapping exercise to advance clinical translation of photoacoustic imaging: from current barriers to future adoption. *Photoacoustics* **32**, 100539 (2023).
203. Beswick, D. M. et al. Biomedical device innovation methodology: applications in biophotonics. *J. Biomed. Opt.* https://doi.org/10.1117/1.JBO.23.2.021102 (2017).
204. Marcu, L., Boppart, S. A., Hutchinson, M. R., Popp, J. & Wilson, B. C. Biophotonics: the big picture. *J. Biomed. Opt.* https://doi.org/10.1117/1.JBO.23.2.021103 (2017).
205. Popp, J., Matthews, D., Martinez-Coll, A., Mayerhofer, T. & Wilson, B. C. Challenges in translation: models to promote translation. *J. Biomed. Opt.* https://doi.org/10.1117/1.JBO.23.2.021101 (2017).
206. Gröhl, J., Hacker, L. & Cox, B. Photoacoustic data and device parameters. *IPASC* https://www.ipasc.science/wp-content/uploads/2023/01/20210916_IPASC_Format_V2.pdf (2021).
207. Gröhl, J. et al. The IPASC data format: a consensus data format for photoacoustic imaging. *Photoacoustics* **26**, 100339 (2022).
208. Deng, H., Qiao, H., Dai, Q. & Ma, C. Deep learning in photoacoustic imaging: a review. *J. Biomed. Opt.* **26**, 040901 (2021).
209. Yang, C., Lan, H., Gao, F. & Gao, F. Review of deep learning for photoacoustic imaging. *Photoacoustics* **21**, 100215 (2021).
210. Grohl, J., Schellenberg, M., Dreher, K. & Maier-Hein, L. Deep learning for biomedical photoacoustic imaging: a review. *Photoacoustics* **22**, 100241 (2021).
211. Vogt, W. C. Proposed list of terms and definitions. *IPASC* https://www.ipasc.science/wp-content/uploads/2023/01/20191210_Terms_Definitions_For_PAT.pdf (2019).
212. Goodsitt, M. M., Carson, P. L., Witt, S., Hykes, D. L. & Kofler, J. M. Jr. Real-time B-mode ultrasound quality control test procedures. Report of AAPM Ultrasound Task Group No. 1. *Med. Phys.* **25**, 1385–1406 (1998).
213. Browne, J. E. Ultrasound elastography special issue. *Ultrasound* https://doi.org/10.1258/ult.2012.012e (2012).
214. Hacker, L. et al. Criteria for the design of tissue-mimicking phantoms for the standardization of biophotonic instrumentation. *Nat. Biomed. Eng.* **6**, 541–558 (2022).
215. Jia, C., Vogt, W. C., Wear, K. A., Pfefer, T. J. & Garra, B. S. Two-layer heterogeneous breast phantom for photoacoustic imaging. *J. Biomed. Opt.* https://doi.org/10.1117/1.JBO.22.10.106011 (2017).
216. Vogt, W. C., Jia, C., Wear, K. A., Garra, B. S. & Pfefer, T. J. Phantom-based image quality test methods for photoacoustic imaging systems. *J. Biomed. Opt.* https://doi.org/10.1117/1.JBO.22.9.095002 (2017).
217. Avigo, C. et al. Organosilicon phantom for photoacoustic imaging. *J. Biomed. Opt.* **20**, 46008 (2015).
218. Cabrelli, L. C. et al. Glycerol-in-SEBS gel as a material to manufacture stable wall-less vascular phantom for ultrasound and photoacoustic imaging. *Biomed. Phys. Eng. Express* https://doi.org/10.1088/2057-1976/ac24d6 (2021).
219. Hacker, L., Joseph, J., Lilaj, L. & Manohar, S. Recommendations for a photoacoustic phantom material. *IPASC* https://www.ipasc.science/wp-content/uploads/2023/06/IPASC-phantom-consensus-document.pdf (2023).
220. Hacker, L. et al. A stable phantom material for optical and acoustic imaging. *J. Vis. Exp.* https://doi.org/10.3791/65475 (2023).
221. Dogan, B. E. et al. Optoacoustic imaging and gray-scale US features of breast cancers: correlation with molecular subtypes. *Radiology* **292**, 564–572 (2019).
222. Zalev, J. et al. In *Photons Plus Ultrasound: Imaging and Sensing 2012* 53–58 (SPIE, 2012).
223. Neuschler, E. I. et al. Downgrading and upgrading gray-scale ultrasound BI-RADS categories of benign and malignant masses with optoacoustics: a pilot study. *AJR Am. J. Roentgenol.* **211**, 689–700 (2018).
224. Seiler, S. J., Neuschler, E. I., Butler, R. S., Lavin, P. T. & Dogan, B. E. Optoacoustic imaging with decision support for differentiation of benign and malignant breast masses: a 15-reader retrospective study. *AJR Am. J. Roentgenol.* **220**, 646–658 (2023).
225. Zalev, J. et al. Opto-acoustic imaging of relative blood oxygen saturation and total hemoglobin for breast cancer diagnosis. *J. Biomed. Opt.* **24**, 1–16 (2019).
226. Food & Drug Administration. *Information for Manufacturers Seeking Marketing Clearance of Diagnostic Ultrasound Systems and Transducers. Guidance for Industry and FDA Staff* 1–64 (FDA, 2008).
227. Ladd, M. E. The medical device regulation and its impact on device development and research in Germany. *Z. für Medizinische Phys.* **33**, 459 (2023).
228. Singh, M. K. A. Cyberdyne, Inc.: CYBERDYNE AcousticX - A new paradigm in photoacoustic imaging. Presented at the SPIE BiOS Exhibition Product Demonstrations (SPIE, 2021).
229. Ntziachristos, V. & Razansky, D. Molecular imaging by means of multispectral optoacoustic tomography (MSOT). *Chem. Rev.* **110**, 2783–2794 (2010).
230. Jüstel, D. et al. Spotlight on nerves: portable multispectral optoacoustic imaging of peripheral nerve vascularization and morphology. *Adv. Sci.* **10**, e2301322 (2023).
231. Karlas, A. et al. Skeletal muscle optoacoustics reveals patterns of circulatory function and oxygen metabolism during exercise. *Photoacoustics* **30**, 100468 (2023).
232. Tsuge, I. et al. Preoperative vascular mapping for anterolateral thigh flap surgeries: a clinical trial of photoacoustic tomography imaging. *Microsurgery* **40**, 324–330 (2020).
233. Matsumoto, Y. et al. Visualising peripheral arterioles and venules through high-resolution and large-area photoacoustic imaging. *Sci. Rep.* **8**, 14930 (2018).
234. Cho, S., Jeon, S., Choi, W., Managuli, R. & Kim, C. Nonlinear pth root spectral magnitude scaling beamforming for clinical photoacoustic and ultrasound imaging. *Opt. Lett.* **45**, 4575–4578 (2020).
235. Lin, L. et al. High-speed three-dimensional photoacoustic computed tomography for preclinical research and clinical translation. *Nat. Commun.* **12**, 882 (2021).
236. Yao, J. et al. Multiscale photoacoustic tomography using reversibly switchable bacterial phytochrome as a near-infrared photochromic probe. *Nat. Methods* **13**, 67–73 (2016).
237. Jeon, S., Choi, W., Park, B. & Kim, C. A deep learning-based model that reduces speed of sound aberrations for improved in vivo photoacoustic imaging. *IEEE Trans. Image Process.* **30**, 8773–8784 (2021).
238. Davoudi, N., Deán-Ben, X. L. & Razansky, D. Deep learning optoacoustic tomography with sparse data. *Nat. Mach. Intell.* **1**, 453–460 (2019).
239. Chlis, N.-K. et al. A sparse deep learning approach for automatic segmentation of human vasculature in multispectral optoacoustic tomography. *Photoacoustics* **20**, 100203 (2020).
240. Zhang, J., Chen, B., Zhou, M., Lan, H. & Gao, F. Photoacoustic image classification and segmentation of breast cancer: a feasibility study. *IEEE Access* **7**, 5457–5466 (2018).
241. Bai, B. et al. Deep learning-enabled virtual histological staining of biological samples. *Light Sci. Appl.* **12**, 57 (2023).
242. Cao, R. et al. Label-free intraoperative histology of bone tissue via deep-learning-assisted ultraviolet photoacoustic microscopy. *Nat. Biomed. Eng.* **7**, 124–134 (2023).

243. Qian, X., Zheng, Y. & Chen, Y. Micro/nanoparticle-augmented sonodynamic therapy (SDT): breaking the depth shallow of photoactivation. *Adv. Mater.* **28**, 8097–8129 (2016).
244. Suzuki, Y. et al. Photoacoustic lymphangiography exhibits advantages over near-infrared fluorescence lymphangiography as a diagnostic tool in patients with lymphedema. *J. Vasc. Surgery Venous Lymphatic Disord.* **10**, 454–462.e1 (2022).
245. Wong, T. T. et al. Label-free automated three-dimensional imaging of whole organs by microtomy-assisted photoacoustic microscopy. *Nat. Commun.* **8**, 1386 (2017).
246. Wong, T. T. et al. Fast label-free multilayered histology-like imaging of human breast cancer by photoacoustic microscopy. *Sci. Adv.* **3**, e1602168 (2017).
247. Zhang, W. et al. Real-time, volumetric imaging of radiation dose delivery deep into the liver during cancer treatment. *Nat. Biotechnol.* **41**, 1160–1167 (2023).

Acknowledgements

The authors' work is supported by the Basic Science Research Program through the National Research Foundation of Korea (NRF) funded by the Ministry of Education (2020R1A6A1A03047902) and the Ministry of Science and ICT (2023R1A2C3004880); by the National R&D Program through the NRF funded by Ministry of Science and ICT (2021M3C1C3097624); by the Korea Medical Device Development Fund grant funded by the Korea Government (the Ministry of Science and ICT, the Ministry of Trade, Industry and Energy, the Ministry of Health & Welfare, the Ministry of Food and Drug Safety) (9991007019, KMDF_PR_20200901_0008); and by the BK21 FOUR project. S.B. is supported by Cancer Research UK (C9545/A29580) and EPSRC (EP/R003599/1). IPASC are supported by EPSRC (EP/V027069/1).

Author contributions

C.K., J.P., S.C., F.K. and B.C. researched data for the article. C.K., J.P., S.C. and F.K. contributed substantially to discussion of the content. C.K., J.P., S.C., F.K. and B.C. wrote the article. All authors reviewed and/or edited the manuscript before submission.

Competing interests

C.K. has financial interests in OPTICHO, which, however, did not support his work. B.C. has financial interests in Seno Medical Instruments, which, however, did not support his work. L.V.W. has a financial interest in Microphotoacoustics, Inc., CalPACT, LLC, and Union Photoacoustic Technologies, Ltd., which, however, did not support this work. F.K. has financial interests in iThera Medical GmbH, which, however, did not support his work. S.B. reports a relationship with iThera Medical GmbH that includes non-financial support. However, it did not support her work. The other authors declare no competing interests.

Additional information

Supplementary information The online version contains supplementary material available at https://doi.org/10.1038/s44222-024-00240-y.

Peer review information *Nature Reviews Bioengineering* thanks Liming Nie, Ivan Pelivanov and the other, anonymous, reviewer(s) for their contribution to the peer review of this work.

Related links

IPASC: www.ipasc.science